

**KEY ISSUES REVIEW**

# Remotely controlled fusion of selected vesicles and living cells: a key issue review

To cite this article: Azra Bahadori *et al* 2018 *Rep. Prog. Phys.* **81** 032602

View the [article online](#) for updates and enhancements.

## Key Issues Review

# Remotely controlled fusion of selected vesicles and living cells: a key issue review

Azra Bahadori, Guillermo Moreno-Pescador, Lene B Oddershede<sup>✉</sup>  
and Poul M Bendix<sup>✉</sup>

Niels Bohr Institute, University of Copenhagen, Blegdamsvej 17, 2100 Copenhagen, Denmark

E-mail: [bendix@nbi.ku.dk](mailto:bendix@nbi.ku.dk)

Received 12 January 2017, revised 20 October 2017

Accepted for publication 9 November 2017

Published 25 January 2018



CrossMark

Corresponding Editor Professor Masud Mansuripur

## Abstract

Remote control over fusion of single cells and vesicles has a great potential in biological and chemical research allowing both transfer of genetic material between cells and transfer of molecular content between vesicles. Membrane fusion is a critical process in biology that facilitates molecular transport and mixing of cellular cytoplasm with potential formation of hybrid cells. Cells precisely regulate internal membrane fusions with the aid of specialized fusion complexes that physically provide the energy necessary for mediating fusion. Physical factors like membrane curvature, tension and temperature, affect biological membrane fusion by lowering the associated energy barrier. This has inspired the development of physical approaches to harness the fusion process at a single cell level by using remotely controlled electromagnetic fields to trigger membrane fusion. Here, we critically review various approaches, based on lasers or electric pulses, to control fusion between individual cells or between individual lipid vesicles and discuss their potential and limitations for present and future applications within biochemistry, biology and soft matter.

Keywords: plasmonic heating, optical trapping, giant plasma membrane vesicle (GPMV), giant unilamellar vesicle (GUV), gold nanoparticle (GNP), electrofusion, membrane fusion

(Some figures may appear in colour only in the online journal)

## Contents

1. Introduction.....	2	2.2.1. Toxic effects induced by laser irradiation.....	7
1.1. Overview of the techniques for mediating fusion.....	2	2.3. Optically controlled pairing of cells and vesicles .....	8
1.2. Membrane fusion .....	3	2.4. Fusion by using nano-scale plasmonic heaters .....	8
1.3. Applications of controlled cell and vesicle fusion .....	4	3. Optically controlled nano-heaters induce membrane	
1.3.1. Mixing of genes by formation of hybrid		fusion.....	9
cells.....	4	3.1. Interaction between light and metal	
1.3.2. Reprogramming of cells by fusion with stem		nanoparticles .....	10
cells.....	4	3.1.1. Absorption of light induces heating.....	10
1.3.3. Vesicle fusion.....	5	3.1.2. Quantification of heating.....	10
2. Electromagnetic fields for manipulating membranes .....	5	3.1.3. Optical trapping of metal	
2.1. Electrofusion of vesicles and cells .....	5	nanoparticles.....	11
2.2. Fusion induced by pulsed lasers .....	6	3.2. Fusion between synthetic vesicles (GUV–GUV	
		fusion).....	12
		3.2.1. Content and lipid mixing.....	13

3.3. Cell-GUV fusion.....	14
3.4. Cell–cell fusion .....	15
4. Applications of optically mediated membrane fusion.....	16
4.1. Triggering protein binding by controlling membrane composition .....	16
4.2. Fusion of GPMVs to artificial membrane vesicles .....	16
4.3. Transfer of bio- and inorganic materials between cells and vesicles.....	17
5. Discussion .....	18
5.1. Mechanism of fusion.....	19
5.2. Cell pairing.....	21
6. Summary and future directions.....	21
Acknowledgments.....	21
References.....	21

## 1. Introduction

In living organisms, the ability to fuse membranes is critical for morphogenesis, proliferation and for survival of the organism. Fusion of membranes is essential in nano-scale processes like synaptic transmission or viral infection [1], but also on larger scales a number of important processes rely on cell–cell fusion, for example, the fusion between an oocyte and a sperm cell and the regeneration process of tissue [2]. From a biomedical or applicational point of view a method for controlling fusion of membranes holds a great potential for genetic manipulation of cells. Introduction of genetic material into selected cells allows for influencing or controlling cellular regulation, a necessary step for gene therapies. Methods for inducing membrane fusion are also useful in fundamental research. Fusion of membranes, containing reconstituted proteins, can be used in studying membrane and protein biophysics [3, 4] or to facilitate small-scale chemistry [5]. Similarly, creation of hybrid cells by controlled fusion allows investigation of novel hybrid cells inheriting the properties of two different parental cell types. This line of research has received a lot of attention recently due to its enormous potential in terms of reprogramming of somatic cells by fusion to stem cells [6–9]. For these reasons, significant efforts have been made to develop methods for fusing cells or other structures surrounded by membranes.

### 1.1. Overview of the techniques for mediating fusion

Optically controlled fusion is based on the interaction between electromagnetic fields and biomembranes. The most common method in which light has been used to fuse cells is electrofusion where cells or vesicles are exposed to an electric field, for instance in the form of an AC field followed by a DC pulse which causes cells to fuse to other cells or to vesicles [10]. This type of fusion gives rise to an unspecific fusion where any membrane surrounded structure might fuse with another, but without control over exactly which cell or vesicle is about to fuse. This method can be combined with the use of a microfluidic chamber where two or more cells or vesicles can be hydrodynamically trapped and thereby allowing different

cell types to be fused [11]. It is, however, difficult to control exactly which two entities end up in the microfluidic trap on the chip.

An alternative strategy for mediating fusion of vesicles or cells has been to use pulsed lasers with a well-defined wavelength, focal area and power. Laser light in the visible regime is absorbed by biological tissue and in the microwave regime light is absorbed by water. Absorption by biological tissue may lead to cascades of photochemistry which can be rather harmful to the biological tissue and absorption by water leads to a substantial heating of the entire irradiated volume. Certain fusion techniques are based on an ablation, or scissoring, of cells by irradiating a cell population in a medium with high power pulsed UV lasers [12, 13].

In the near-infrared (NIR) regime, with wavelengths between 800 nm and 1100 nm, there is a biological transparency window [14]. In this range light is not absorbed much neither by biological tissue nor by water, and therefore this spectral range provides an optimal window for optical fusion techniques where the aim is to retain a viable biological structure after fusion. Lasers are available with high laser powers, well defined beam profiles, and at a reasonable cost in this wavelength regime. Altogether, these factors make NIR lasers a good choice for optical manipulation of living specimen [15, 16].

Optical trapping of living cells has proven useful for controlled fusion of selected cells and vesicles. In its simplest implementation, an optical trap consists of a tightly focused laser beam which pulls objects with a higher index of refraction than the surrounding media towards the focus. Optical traps based on NIR lasers are relatively harmless to biological specimens if the laser power and duration of trapping are minimized. For instance, yeast cells have been shown to proliferate in a NIR optical trap [16], and trapped bacteria retain their flagellar motion [17] and their ability to maintain a proton gradient across the cell wall [18]. Finally, optical tweezers have been routinely used to probe the physical environment within mammalian cells without any detrimental effects on cell viability [19] and hence is usually considered a safe tool for positioning cells in fusion assays.

Fusion of selected cells has also been realized by combining pulsed lasers with optical trapping. The trap was used to bring the cells of interest close together and then a pulsed UV laser was focused at the contact zone to mediate the fusion [20]. In another implementation, optical tweezers were used to trap the vesicles [21] or cells of choice and bring them into contact. Subsequently, a metallic nanoparticle was trapped in the contact zone between the vesicles [4] or cells [22]. The metallic nanoparticle absorbed part of the light and released the energy in the form of heat thereby triggering a full fusion of the membrane structures and cargos of the cells or vesicles [4, 22].

Optical traps based on a single laser beam are useful for manipulation of individual cells. By splitting a single laser beam into its two orthogonal polarizations by means of a beam splitter cube it is relatively simple to form an optical trapping platform with two individually controllable traps [23], and this allows selection and positioning of two cells in a sample for fusion. However, to mimic an *in vivo* environment

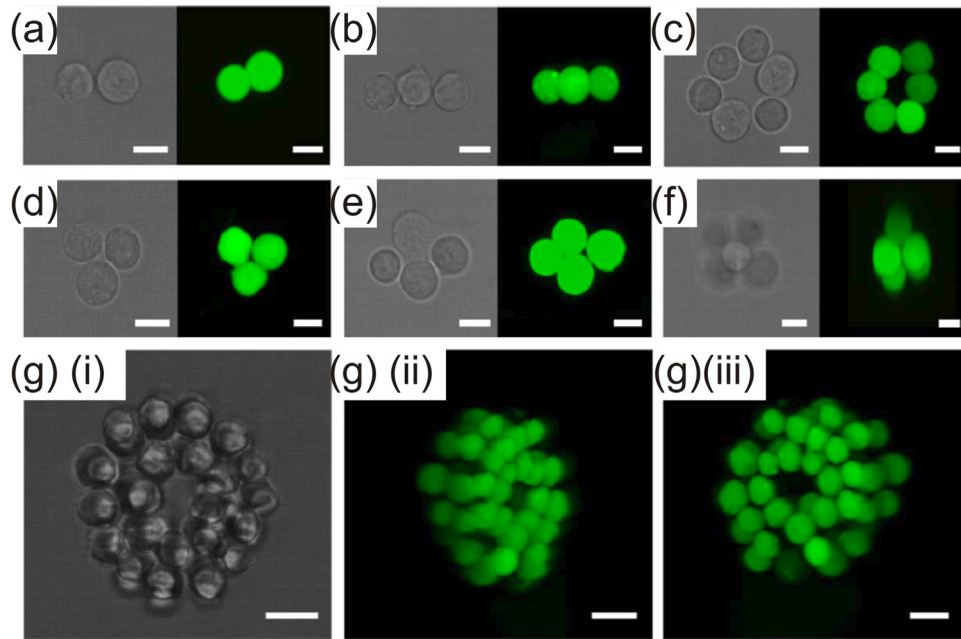


**Figure 1.** Mouse embryonic stem cells arranged into well-controlled 3D structures using holographic optical tweezers. The structures were stabilized using specific biotin–avidin bonds ((a)–(f)) or by implementing them in a PEG based modular hydrogel matrix (g) (i)–(iii). Reproduced from [26]. [CC BY 4.0](#).

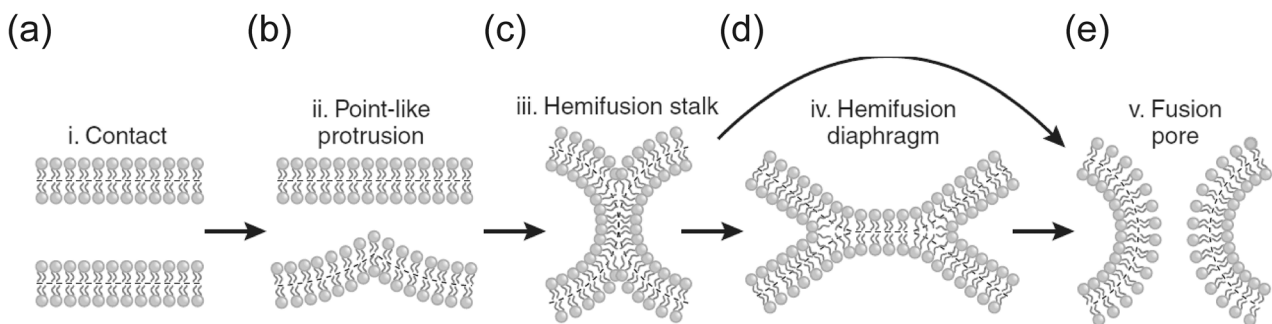


**Figure 2.** Possible intermediate membrane configurations for two membranes during fusion. (a) and (b) Membranes have to be in close proximity to initiate fusion. (c) Fusion of the proximal leaflets will cause lipid mixing between the two initially separated membranes. (d) Extension of the hemifused diaphragm causes the distal leaflets to come closer together to form a bilayer. (e) Formation of the fusion pore completes fusion. Reprinted by permission from Macmillan Publishers Ltd: Nature Structural & Molecular Biology [28], Copyright (2008).

with multiple cells arranged in a 3D pattern it is an advantage to manipulate more than two cells. This can be done by holographic optical tweezers [24] which are achieved by passing the laser beam through a computer generated hologram, in practice most often realized by means of a spatial light modulator (SLM). By the generalized phase contrast (GPC) technique one can create arbitrary trapping patterns by the SLM without explicitly calculating the holograms and therefore, this is highly efficient [25]. One example where holographic optical tweezers are used to arrange embryonic stem cells in a well-defined 3D structure is shown in figure 1 [26]. After assembly the structures were stabilized by specific cell–cell adhesion bonds or by assembling the structures in a solidifying hydrogel. This kind of cellular arrangement is highly desirable for understanding the influence of cell–cell communication or could be useful for creating fused structures based on a large number of cells.

## 1.2. Membrane fusion

Cells are surrounded by membranes, and for two cells to mix their membranes and their cytoplasms they must undergo a full fusion of both the outer and inner leaflet of the membranes constituting the barrier between the interior and the exterior of the cell. Because of an energetic barrier, two membranes in close proximity will not fuse spontaneously, and natural cell fusion is usually mediated by proteins that lower this energy barrier [27]. In the synaptic region, the membrane fusion barrier is overcome by SNARE protein complexes (calcium-triggered soluble N-ethylmaleimide-sensitive-factor attachment protein receptor) [1].

The physical techniques for mediating fusion, discussed in this review, provide the necessary energy for overcoming the energetic barrier for merging two membranes. However, care must be taken to not misinterpret an uncomplete fusion with a full fusion. Some possible intermediate steps involved

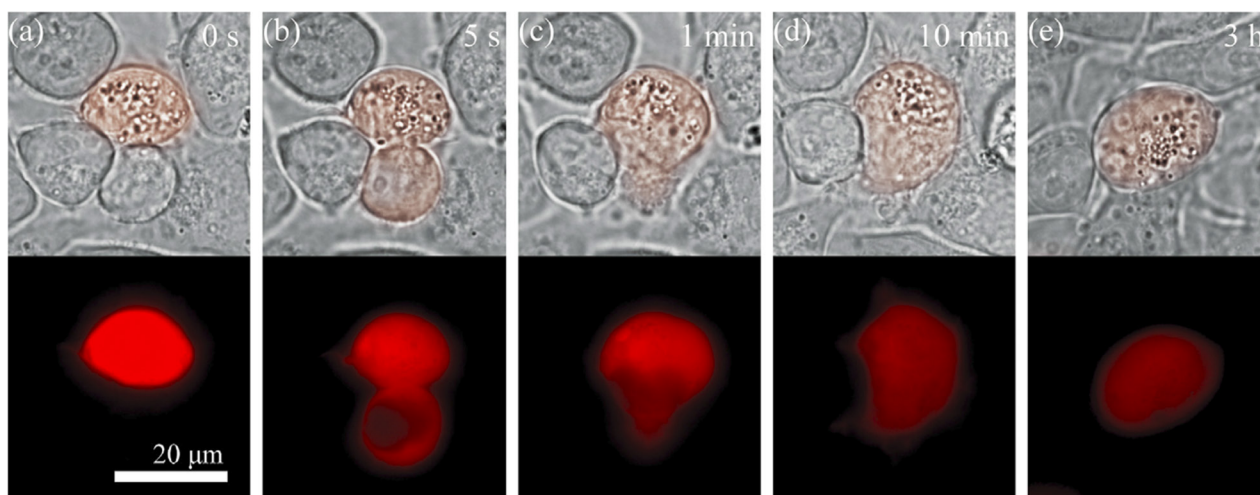


**Figure 3.** A hESC is optically fused to a mCherry labeled primary HDFn. The two cells were brought into contact by an optical trap based on a NIR laser and then a UV pulsed laser was used as an optical scissor to create a hole in the cell surfaces at the contact zone thereby mediating a full fusion. Reprinted with permission from [20]. Copyright (2013), AIP Publishing LLC.

in merging two membrane bilayers of a cell or a vesicle are depicted in figure 2 [28]. During fusion the membranes can form a hemifused intermediate state (c) in which the two membranes can experience lipid mixing, but without mixing of the interior content. As will be shown in the following sections, these two cases can be experimentally distinguished by using a fluorescent marker for the aqueous lumen and a different one for the membrane.

A full fusion of cells or vesicles is therefore accomplished once their internal proteins and cytosol solution are properly mixed and a method for fusion has to be tested with regard to content mixing prior to considering applications with the technique. We note, however, that here we define two cells to be fused once the cytosols are mixed and the fused structure contains one or two nuclei, i.e., the genetic material encapsulated within the nuclei might not mix within the hybrid cell.

### 1.3. Applications of controlled cell and vesicle fusion

The ability to control cell and vesicle fusion allows for the delivery of chemical and biological factors to living cells. If DNA or RNA are delivered to a selected cell, this will allow for viral replication or for performing gene silencing, thereby affecting the fate and function of the specific cell. From a research point of view, controlled fusion of living cells also gives access to study genetic changes that are inherited by the fusion of two different cells. As methods for fusing two selected cells were only recently developed, not many examples of successful formation of hybrid cells yet exist, but a few of examples are given in the sections below.

**1.3.1. Mixing of genes by formation of hybrid cells.** The creation of functional hybrid cells is the backbone of hybridoma technology which is primarily used for production of antibodies in large amounts. The two cells which are fused are a white blood cell, a B cell that produces the desired antibodies, and an immortal cancer cell. This new hybrid cell now has the ability to produce the correct antibody in a large amount and

retains the immortality of the cancer cell. The hybridomas can be grown in culture whereafter the monoclonal antibodies can be harvested in large amounts. This method of producing monoclonal antibodies [29] was invented by Milstein and Köhler and awarded the Nobel Prize in 1984.

**1.3.2. Reprogramming of cells by fusion with stem cells.** Stem cells are undifferentiated cells that have the capacity to self-renew or to develop into any specialized cell of the organism. Therefore, stem cells have enormous potential for personalized medicine and huge efforts are being put into understanding how to control stem cell development. If pluripotent stem cells are produced from the somatic cells of an individual, then these cells can in principle be used to relieve pathologies of the individual without being rejected by the immune system. For this reason, efforts are being made to produce induced pluripotent stem cells (iPSCs) from somatic cells. There are at least two ways to produce iPSCs from somatic cells [30], one of these involves the transfer of a somatic cell nucleus to an egg cell that has its own nucleus removed and then a clone will be made of the individual from whom the somatic cell came [31]. Another way to produce iPSCs is to introduce, for instance by viral infection, four essential transcription factors into somatic cells. This method was first reported by Takahashi and Yamanaka [32] using mouse embryonic fibroblasts and was awarded the Nobel prize in 2012. It is currently debated in literature which of the two methods has the largest potential for clinical applications, but in common for both methods is the fact that they rely on fusion of somatic cells with another cell or with a viral capsid or some other carrier of transcription factors like for example a liposome.

Optically mediated fusion of selected human embryonic stem cells (hESCs) and of hESCs with somatic cells was first reported by Chen *et al* [20]. Two cells, hESCs or primary human dermal fibroblasts (HDFns), were selected by a holographic optical tweezers system and brought into contact. A pulsed UV laser with wavelength of 355 nm was then focused at the contact zone and fusion occurred. Figure 3 shows an

example of fusing a hESC to a HDFn (cytoplasm labeled red), successful fusion is observed by transfer of the cytoplasmic dye from the HDFn to the fused structure. Also, the fused structure was shown to remain viable.

Cellular reprogramming by electrofusion of mouse embryonic stem cells with mouse embryonic fibroblasts was demonstrated in [33]. Fibroblasts were successfully reprogrammed using stem cells for reactivation of a latent embryonic gene (GFP-OCT-4) which was inactive in the unfused fibroblasts, but could be activated by fusion with embryonic stem cells. This result shows that cellular reprogramming can be studied by using remotely controlled fusion of cells.

**1.3.3. Vesicle fusion.** Biophysical research of reconstituted biological systems has also benefited greatly from the tools invented by the optical community. Self-assembled membrane systems like supported lipid bilayers (SLBs) or membrane vesicles are highly amenable for manipulation with focused laser beams or electric pulses [4, 5, 21, 23, 34–37]. Optical techniques for membrane manipulation are particularly useful if applied together with the diverse array of biochemical techniques available today for making vesicles containing proteins in the lumen [38, 39] or in the membrane [40]. Examples of such applications includes chemical or biochemical reactions triggered by optical fusion of vesicles containing different chemical/biological environments [4, 36, 37]. In this review we also discuss how giant plasma membrane vesicles (GPMVs), extracted from living cells, can be optically fused to synthetic vesicles. This approach opens up unexplored applications in which reconstitution of the cytoskeleton could be possible by transferring proteins like actin or microtubule monomers into the cytosol-like environment of the GPMV where all polymerization factors should be present as well as membrane proteins which may interact with the cytoskeleton.

The power of optical techniques in the context of fusion is not limited to membranes and cells. Laser induced fusion of micrometer sized spherical polymer capsules doped with gold nanoparticles (GNPs) was recently shown in [41]. This application confirms that optics can be used as a general tool for manipulating and fusing both living and soft matter with additional areas of applications likely to emerge in the near future.

In the following, we first review the use of electromagnetic fields (electric pulses and pulsed lasers) for fusion of cells and vesicles. This is followed by a review of the use of plasmonic heating of metallic nanoparticles to mediate membrane fusion. The different types of fusion fall into three categories involving (i) fusion of two or several living cells, (ii) fusion of a living cell with a vesicle or (iii) fusion of two vesicles. The review is concluded by presentation of a few examples which demonstrate the usefulness of the fusion strategies.

## 2. Electromagnetic fields for manipulating membranes

The use of electromagnetic fields for disrupting cell membranes and for manipulating cells allows for the ultimate remote control for regulation of the cellular cytoplasm. This can now be accomplished by using electrofusion or pulsed

lasers for selective cell–cell fusion or fusion of cargo vesicles with cells. Spontaneous fusion of two biological membranes rarely occurs due to an energy barrier associated with disrupting and merging two membranes. In absence of Nature's own machinery of special fusion proteins, the external energy needed for mediating fusion can be supplied by an electric field. Here, we discuss the different methods by which electromagnetic fields have been used for inducing fusion by either application of electric pulses, by focused pulsed lasers, or by irradiation of absorbing nanoparticles at the contact region between membranes.

### 2.1. Electrofusion of vesicles and cells

Electrofusion has been extensively used for mediating fusion between cells and vesicles. Application of DC electric pulses generates a high transmembrane potential which can porate membranes. Electroporation has been exploited for fusion of vesicles and cells including fusion of different cell types with vesicles [5, 10, 11, 37, 42–47].

The poration of membranes in response to electric pulses was studied in detail in [37] where the timescales associated with electrofusion of GUVs were quantified (see figure 4(a)). The rate of expansion of the fusion pore was measured, see figure 4(b), by a high-speed camera. Two rates of expansion were detected, the first expansion from nanometers to a few micrometers occurred within milliseconds at a rate of expansion of centimeters per second after which the expansion slowed down due to relaxation of membrane tension. After  $\sim 1$  s the expansion again increased until the structure became more spherical, see figure 4(b).

Electrofusion is generally perceived as a relatively gentle technique which does not damage biological molecules or significantly harm living cells and this method has indeed also been extended to fusion of living cells for forming viable fused cells [33, 42–47]. The efficiency of fusion has been found to increase with increasing voltage up to  $\sim 1.6$  kV cm<sup>-1</sup>, however, with a concomitant decrease in cell viability [47].

The application of a uniform field within a microscope chamber exposes all cells to the DC pulse and hence, the method does not provide selectivity in terms of which cells to fuse. However, Stromberg and coworkers performed electrofusion locally to a pair of cells using microelectrodes attached to the respective cells [48]. Additionally, the cells in this study were brought together by using a NIR optical trap, thus providing complete specificity over which cells to fuse. The elaborate and slow work of combining microelectrodes with optical trapping is technically challenging and only simple imaging was implemented in this study to monitor the fusion process for indicating viability.

To increase the throughput for fusion of cells and vesicles, the electrofusion technique was implemented in combination with novel microfluidic strategies for pairing a large number of cells. Pairing different types of cells was achieved by flowing cells through an array of microstructured 'cups' which acted like cell traps. By loading the two cell types sequentially into the device, proper cell pairing of differently labeled cell types was accomplished, see figures 5(a)–(d) [33].

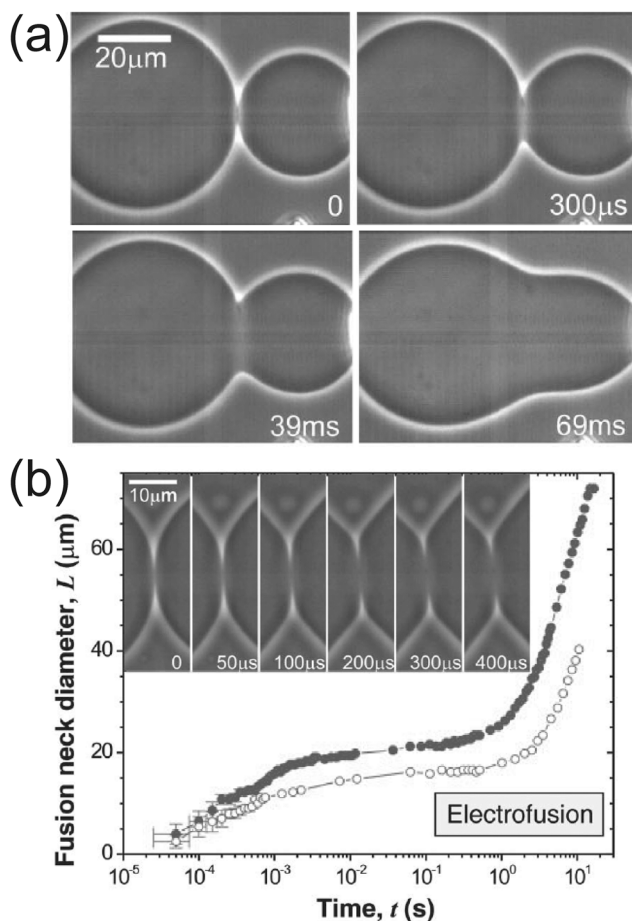


**Figure 4.** Electrofusion of GUVs. (a) Application of a DC electric pulse induces fusion of GUVs. The evolution of the fusion pore is monitored by high-speed camera acquisition using transmitted light imaging. (b) The diameter of the fusion pore increases with a rate of  $\sim 4 \text{ cm s}^{-1}$  during the initial phase. The rate of expansion then slows down in the interval 1 ms to 1 s, after which the rate of expansion again increases. The two different symbols represent examples of two different fusion events. Reproduced with permission from [37]. Copyright © 2006 National Academy of Sciences.

As an interesting application of this device, cellular reprogramming by fusion of mouse embryonic stem cells with mouse embryonic fibroblasts was demonstrated, as shown in figure 5(h). Reactivation of a latent embryonic gene (GFP-OCT-4, green color in figure 5(h)) which was inactive in the unfused fibroblasts, but could be activated by fusion with embryonic stem cells. The uniform expression of GFP-OCT-4 in figure 5 results from selection of fused cells containing inherited drug resistance from the two unfused populations.

The fusion efficiency using electrofusion obviously depends on how efficiently the cells are paired. The maximum cell pairing efficiency was 80% (percentage of traps occupied by two cells of any type) whereas different cell types were paired with up to 70% efficiency (percentage of traps occupied by two cells of different type). Subsequently, application of an electric field resulted in a fusion efficiency of up to 78%. After application of the field sorting of the cells was not performed and the collection of cells from this device consisted of both fused and unfused cells. However, the fused cells were

monitored by cytoplasmic labeling of cells with red and green fluorescent markers which allowed fused cells to be distinguished with a red–green color overlap. Examples of apparently live cells 4 days after fusion are shown in figures 5(e) and (f), but no statistical data on viability were provided and no strict viability test was applied.

Microstructures are efficient tools for massive positioning of a large number of cells and in addition allow the fluid to be exchanged while the cells stay paired and registered. The device presented in figure 5 has a great potential as a high throughput fusion device if combined with a cell sorting system for harvesting the viable hybrid cells. Cell sorting has been integrated into microfluidic devices by using image recognition to identify cell characteristics and subsequently controlling the flow direction of selected cells into specific compartments using an optical trap [49].

In most studies with electrofusion of cells, a hypotonic medium is used to swell the cells thereby rounding up the cells and stretching the plasma membranes. The effect of osmolarity has been systematically investigated and was found to critically influence the voltage which is necessary to induce fusion. By investigating the fusion yield between B16-F1 cells it was found that fusion was amplified in a hypotonic buffer [50]. The application of an electric field on cells suspended in a non-physiological environment, like a hypotonic sugar solution, has to be performed with care, but cell tracking over several days shows that significant levels of cell survival can be achieved in such approaches [33].

## 2.2. Fusion induced by pulsed lasers

Pulsed lasers have been successfully used to fuse different cell types ranging from mammalian cells [12, 20, 51–54] to plant cells [13]. The high focal intensity resulting from tight focusing and high intensity femtosecond (fs) peaks efficiently ionizes biological tissue, which can lead to optical breakdown of dielectric material. Focusing a femtosecond laser onto the contact area between two cells can result in immediate local membrane rupture and merging of the two cells (see figure 6).

The use of pulsed lasers has a long history of use in topics closely related to biological fusion, namely in nanosurgery, and in cutting and ablation of both mammalian and plant cells [13, 56]. Additionally, femto-second (fs) pulsed lasers were recently used for disrupting cell membranes to achieve successful transfection of neurons [57]. The mechanism behind fs induced laser ablation relies on optically induced ionization of the biological material causing local membrane rupture at the focal spot [56].

A high penetration depth in tissue is achieved with pulsed NIR lasers [14] and additionally allows two-photon imaging of the cells [58]. UV pulsed lasers are not suitable for thick specimens due to poor penetration, but have the advantage of a smaller focal spot diameter which can be utilized for inducing highly localized perforation [20]. The strongly nonlinear two-photon absorption makes the likelihood of simultaneous absorption of two photons very low except at the focus where the intensity is highest. For Gaussian shaped beam profiles

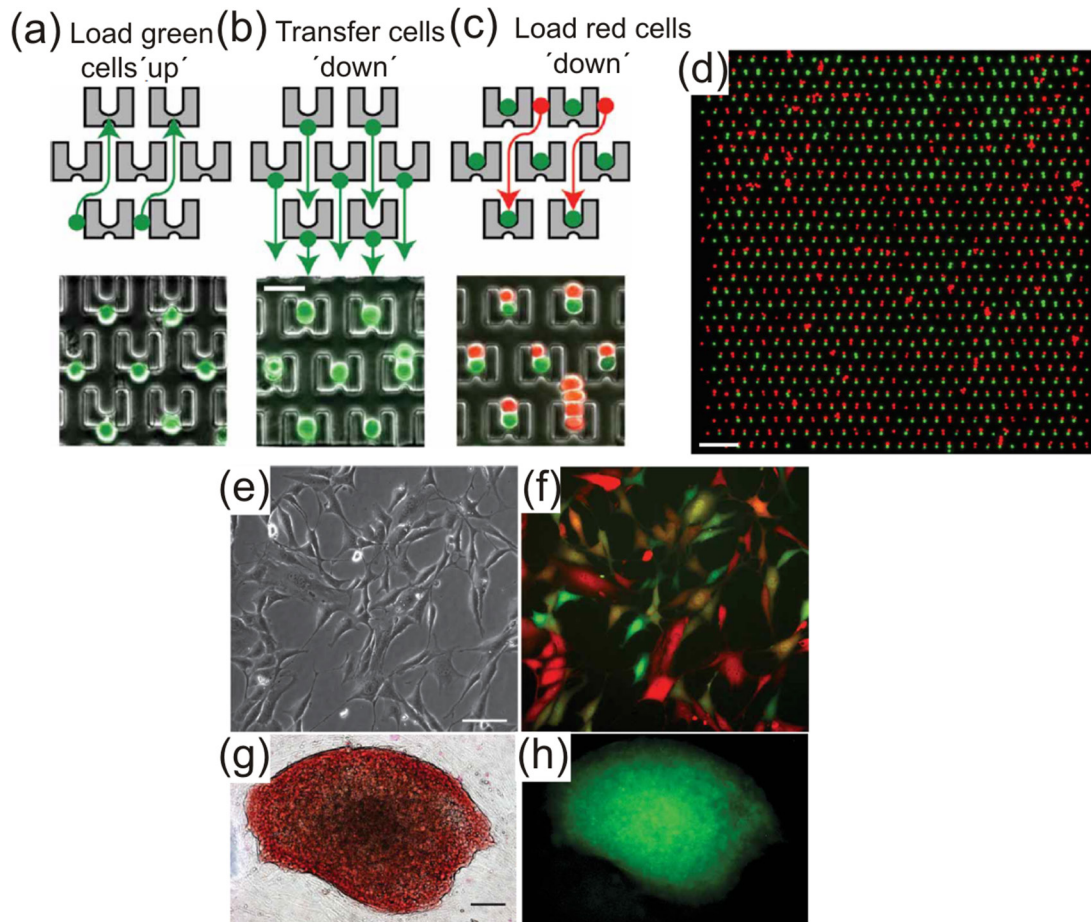


**Figure 5.** Microstructured array for pairing cells for electrofusion. (a)–(c) Microstructured cups are able to trap cells flowing in a specific direction (downwards in the images). (a) First, cells can be loaded into the device with an opposite flow direction (upwards in the images) which traps the cells on the backside of the cups. (b) Then the flow is reversed to confine the cells within the cup. (c) Cells become paired by first loading and trapping the green-labeled cells, followed by sequential loading and trapping of red-labeled cells. The bottom row shows fluorescent images of several cell pairings and in (d) a larger fraction of the array shows ~1000 cell pairing events. (e) and (f) Viability of electrofused 3T3 cells shown after 4 d. Cells are labeled with DsRed and eGFP, respectively. The red–green labeled cells are hybrids. (g) and (h) Reprogramming of mouse embryonic fibroblasts (mEF) cells by mouse embryonic stem (mES) cells demonstrated by reactivation of embryonic gene Oct4 (green in (h)). The images show a 14 d old colony of hybrids having double drug resistance inherited from fused mES cell and mEF cells, respectively. The red color in (g) is alkaline phosphatase activity, indicating cell viability, and the green color in (h) is a Oct4-GFP reporter initially inside the mEF cells and which was activated after fusion with mES cells. Scale bar 50  $\mu\text{m}$  (b) and 200  $\mu\text{m}$  (d). Reprinted by permission from Macmillan Publishers Ltd: Nature Methods [33], Copyright (2009).

the strong nonlinearity of the absorption also permits a region to be ionized which is smaller than the diffraction limit since absorption mainly occurs near the central part of the Gaussian intensity peak.

**2.2.1. Toxic effects induced by laser irradiation.** The high intensity delivered by pulsed lasers produces tangible and noxious side effects when focused into living cells. The most important effects associated with high intensity fluxes include (i) formation of gaseous bubbles with radii of ~200 nm (for fs lasers) [56] or larger, depending on the laser intensity and the pulse duration and repetition rate, (ii) formation of an electron plasma which contributes significantly to creation of toxic reactive oxygen species (ROS) [59–61]. For these reasons it is critically important to find appropriate irradiance levels which are sufficient to restructure membranes, but which are still low enough to minimize formation of ROS. The effect

of ROS generated by fs pulsed lasers, used for cell poration, was investigated in [61]. Clear evidence of increased levels of ROS was found in cells exposed to fs pulsed laser irradiation including laser-induced effects on DNA strand breakage, structural deformation, fragmentation of the membrane and the cells' nucleus (see figure 7).

The pulse energy required to generate a plasma ablation depends on the wavelength, the focusing ability of the setup, and the pulse duration. For nanosecond pulsed lasers the pulse energy required to facilitate fusion is of order of  $\mu\text{J}$  whereas for picosecond pulses the threshold energy becomes much lower and for femtosecond laser ablation the threshold energy is on the order of nJ [20, 54, 62]. The lower pulse energy of fs lasers makes them much more appropriate for fusion since the cavitation shock waves are smaller and hence less destructive.

A comparative investigation between ROS generation from CW and pulsed Nd:YAG ( $\lambda = 1064\text{ nm}$ ) lasers was performed

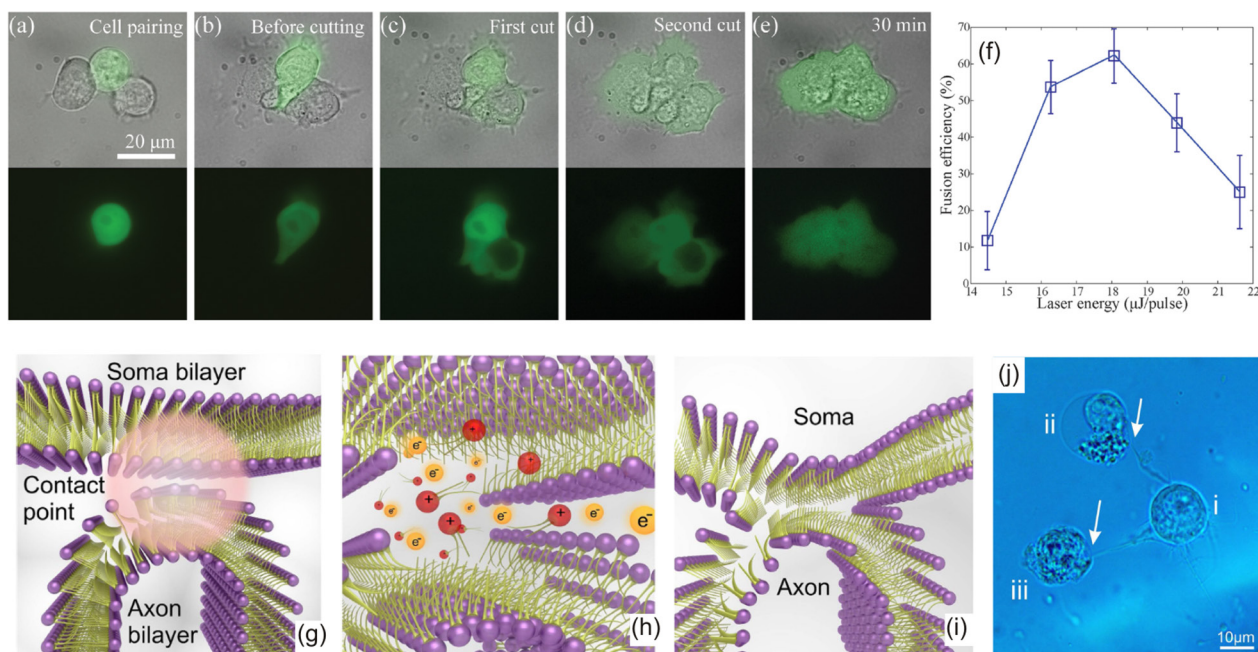


**Figure 6.** Cellular fusion and hemifusion induced by a pulsed laser focused on the intermembrane contact region. (a)–(e) Cell pairing and fusion of three hESCs. The cell pairing was performed using an optical trap and subsequently fusion was induced by UV (355 nm) nanosecond laser pulses. Spreading of cytoplasmic GFP reveals fusion and is sequentially triggered by irradiating the two contact areas joining three cells resulting in a hybrid cell encapsulating the material from three cells. (f) Fusion efficiency by using nanosecond pulses versus pulse energy. (g) Schematics showing a femtosecond laser focused on the contact area joining an axon and soma bilayer. (h) The laser pulses generate a plasma which breaks the lipid molecules forming the bilayer structure. (i) After irradiation the bilayers can seal to form a hemifused structure. (j) Image of three neuronal cells joined by using fs laser pulsed irradiation. ARROWS point at the location of the hemifused junctions. ((a)–(f)) Reprinted with permission from [20]. Copyright (2013), AIP Publishing LLC. ((g)–(j)) Reproduced from [55]. CC BY 4.0.

in [60] (see figure 8). Irradiation of HeLa cells by pulsed laser light resulted in an increase in ROS generation immediately after exposure and ROS generation increased during 10 min of exposure after which it showed a slight decrease, see figure 8. Increasing the pulse energy from 120 μJ to 200 μJ at 10 Hz, predictably resulted in more ROS generation. The ROS formation resulting from pulsed laser irradiation was compared with ROS formation from CW laser light ( $\lambda = 1064$  nm) at 200 mW, see figure 8(b). Irradiation by CW laser light at this power resulted in significantly lower ROS formation. The ROS species were identified to be hydroxyl radicals by testing with quenchers of singlet oxygen (sodium azide) and hydroxyl radicals (mannitol).

These results show that pulsed lasers should be employed for fusion with great care to avoid toxic effects from excessive amounts of ROS. By using lower energy pulses and ROS quenchers these effects can be minimized. Near infrared CW lasers, on the other hand, are relatively harmless to cells and can safely be used for optical trapping and positioning of cells next to each other prior to fusion.

### 2.3. Optically controlled pairing of cells and vesicles

Laser induced fusion can be conveniently combined with optical trapping on the same optical platform by aligning a continuous wave NIR laser through the same objective as demonstrated in [20, 60]. The selectivity of fusion can hence be accomplished through optical trapping and pairing

of individual cells or vesicles. Optical trapping of cells has been demonstrated in different trapping geometries facilitating either multiple traps [26] or a single trap [22]. Stable trapping of vesicles is most effective when a dense solution like sucrose is encapsulated inside the vesicles [4]. This raises the dielectric constant of the interior solution and makes the trapping of a vesicle similar to trapping a spherical dielectric particle [21]. By focusing the optical trap onto the membrane itself, which has a higher dielectric constant than water, vesicles can still be manipulated to some degree, even when they contain the same solution inside as outside the spherical membrane [63]. The spherical shape and uniform composition of vesicles also permits quantitative characterization of the trapping potential of vesicles with various diameters [21]. Such quantitative characterization is, however, problematic for cells which contain a highly heterogeneous cytoplasm and the trapping strength will depend on the exact location of the optical focus within the cell.

### 2.4. Fusion by using nano-scale plasmonic heaters

High laser intensities are needed to perforate membranes in laser induced fusion experiments, but the necessary intensities can be significantly lowered if an absorptive nanoparticle is located at the contact area joining two apposing membranes. Early experiments showed that irradiation of GNPs conjugated to a membrane were found to cause cell membrane perforation [64]. More recently this strategy was used to fuse different

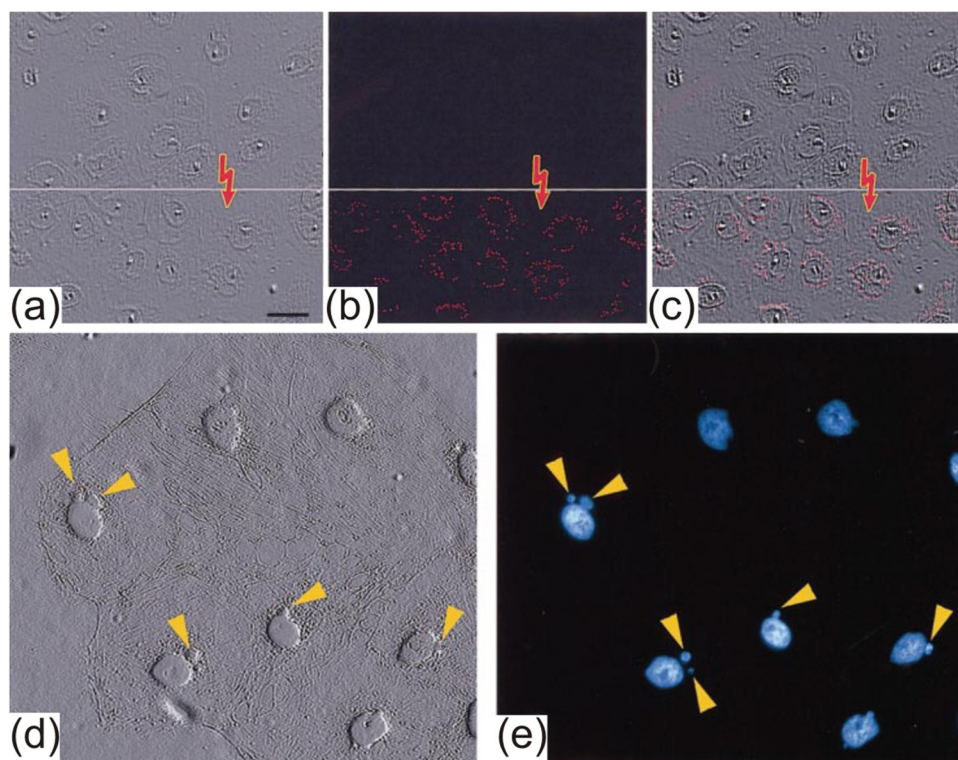


**Figure 7.** Femtosecond laser irradiation generates ROS in cells. (a) Transmitted light imaging of PtK2 cells. (b) Only the cells in lower half of the image were exposed to a high laser power of 7 mW (mean power). The presence of ROS is detected by fluorescence emitted from the fluorescent Jenchrom px blue (red). (c) Overlay of (a) and (b) showing clusters of the Jenchrom px blue reaction product. (d,e) Nuclear blebbing as a result from fs laser irradiation. Selected cells are irradiated and are found to form visible blebs which were visualized in transmitted light (d) and by using nuclear DAPI staining as shown by the blue color in (e). Reprinted from [61], Copyright (2001), with permission from Elsevier.

types of cells [65]. By conjugating two different types of antibodies to the same GNP it was possible to join different cells, expressing different antigens, by using the GNPs as a linker. This cell pairing strategy is shown in figure 9 for dendritic cells (DC) and malignant BJAB (Burkitt lymphoma B) cells.

The use of monospecific anti-EGFR coated GNP conjugated to cells was reported in [66], however, these experiments resulted in very low yield of fusion primarily due to the low affinity for different target cells. In contrast, the particles used in figure 9 have bispecific and high affinity antibodies towards malignant cells and immune cells which resulted in improved pairing of cells. The fusion efficiency of paired cells of different cell types (heterotopic) was 7–9% whereas the fusion efficiency between cells of the same type (homotopic) was 20%. The tight cell adherence junctions, obtained by bispecific antibodies conjugated to GNPs, thus increases the fusion efficiency. Fusion of the cells was triggered by irradiating the GNPs by ten 50 fs laser pulses with a wavelength of 545 nm coinciding closely with the surface plasmon resonance (SPR) of the GNPs at which the absorption is the highest. The mechanism promoting cell fusion in these laser-GNP fusion experiments has not been clarified, but could involve rapid mechanical rupture of the membrane caused by an extremely local and transient absorption of a high intensity light flux.

Recently, a new and related approach involving the use of plasmonic heating of GNPs for triggering fusion was used to fuse both vesicles [4] and cells [22]. This new experimental

method relies on local heating produced by irradiated GNPs which are optically trapped at the contact area between the fusing structures. The use of a CW optical trap to both facilitate cell pairing and fusion makes this approach affordable and highly versatile in terms of selectivity of which cells to fuse. Furthermore, the use of CW near infrared light is known to be practically harmless to cells due to low absorption in the biological material, hence, the potential damage to the cells solely originates from heating of a nanoscale volume surrounding the site of fusion.

In the next section, we describe in detail this hot-nanoparticle-based approach of fusing cells and vesicles. The versatility of this approach is demonstrated by selective cell–cell, vesicle–vesicle, cell–vesicle fusion, but also we demonstrate the feasibility of the method for biophysical studies of membrane proteins by fusing giant plasma membrane blebs (GPMVs) with pure giant unilamellar vesicles (GUVs) having a predefined lipid composition and lumen content.

### 3. Optically controlled nano-heaters induce membrane fusion

Most methods for optically controlled fusion of cells or vesicles rely on a trigger mechanism that is initiated by direct laser irradiation of the cells or vesicles. However, this has certain disadvantages as the light cone, for instance created by a focused pulsed UV laser, will irradiate a relatively large

volume of the sample and might induce severe side effects. Therefore, it is an advantage to utilize a method which only affects a smaller volume, preferably localized only to the contact zone between the two membranes that will be fused. One way of realizing this is to combine the use of absorptive GNPs and an optical trap based on NIR laser light which exhibits low absorption in biological material and water. The plasmonic properties of metallic nanoparticles cause the particles to absorb and dissipate heat from their surface upon irradiation in a highly localized region surrounding the nanoparticle, thus confining thermal damage to a nanoscale region. The absorption spectrum depends on particle size, shape, orientation and material. Nanoparticles with significant absorption in the NIR are commercially available in a high quality, for instance in the form of simple spherical GNPs. In the following, we provide a brief introduction to plasmonic heating of optically trapped metallic nanoparticles. The theory behind the interaction of GNPs with light is discussed and we describe some recent approaches that have been used for measuring the temperature increases in optically trapped GNPs irradiated by NIR light. A brief introduction to optical trapping of metallic nanoparticles is given before we describe the use of optically trapped nano-heaters in fusion.

### 3.1. Interaction between light and metal nanoparticles

**3.1.1. Absorption of light induces heating.** Metallic nanoparticles exhibit strong wavelength dependency in their interaction with light. Peak absorption coincides with the peak in the spectrum of the localized surface plasmons. The absorption of light scales linearly with laser intensity as well as with the absorption cross section of the nanoparticles. The optical cross sections can be calculated for spherical nanoparticles using Mie's equations. The total optical cross section is called the extinction cross section and is given by [67]

$$C_{\text{ext}} = C_{\text{scat}} + C_{\text{abs}} = k^4 |\alpha|^2 / 4\pi + k\alpha'' \quad (1)$$

In equation (1),  $\alpha$  is the complex polarizability and  $\alpha''$  represents the imaginary part of the polarizability,  $k$  is the wave-number given by  $k = 2\pi n/\lambda$  where  $n$  is the index of refraction and  $\lambda$  is the wavelength of light. The normalized extinction changes with particle sizes with a pronounced red shift and broadening for larger particle sizes, as is shown in figure 10. The first part of equation (1) represents the scattering cross section and the second part represents the absorption cross section. The optical cross sections are strongly wavelength dependent (through the polarizability) and for spherical GNPs maximum absorption and scattering is found for wavelengths between 500 and 700 nm. Since  $\alpha$  scales approximately linearly with volume for spherical nanoparticles we see from equation (1) that the scattering cross section scales with square of the volume and the absorption cross section scales with the volume of the nanoparticle. The degree of scattering and heating can therefore be readily controlled through particle size, laser wavelength and laser power.

**3.1.2. Quantification of heating.** The absorption cross sections of nanoparticles and the experimental temperature

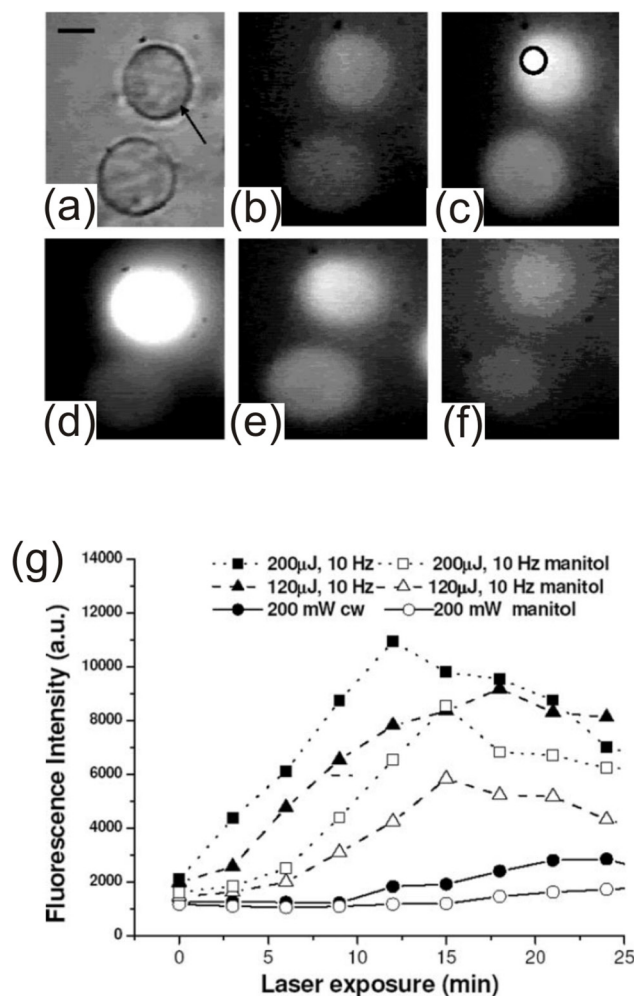


**Figure 8.** ROS formation in HeLa cells after exposure to NIR light (1064 nm) using pulsed or CW lasers. (a) and (b) Bright field and fluorescence image of HeLa cells before exposure to pulsed laser. (c) After 3 min exposure (d) after 12 min (e) after 24 min (f) after 30 min. The cell contains a ROS marker dihydrofluorescein (DCDHF) which produces green light upon ROS formation. (g) Fluorescence intensity of DCDHF as a function of time for different irradiation conditions and in presence (open symbols) or absence of mannitol (filled symbols). Reproduced from [60] with permission of The Royal Society of Chemistry.

increase that results upon irradiation of a nanoparticle have been investigated using different experimental approaches. The small volume of a nanoparticle and the relative localized heat output upon irradiation makes it challenging to directly measure the particle temperature. Instead, the temperature of irradiated nanoparticles has been inferred by using a temperature sensitive matrix surrounding the nanoparticle. In [35] a SLB was used to quantify the temperatures of irradiated GNPs in the size range from 80 to 200 nm. The GNPs were adhered to a gel phase lipid bilayer which locally transformed into a fluid phase bilayer upon irradiation by 1064 nm laser light. The extent of the fluid region was quantified, and using the fact that the temperature decays inversely with distance to the heat source, allowed the surface temperature of the GNP to be extracted. The maximal surface temperature of 100–200 nm GNPs reached above 100 °C during irradiation with 100–200 mW of laser power in

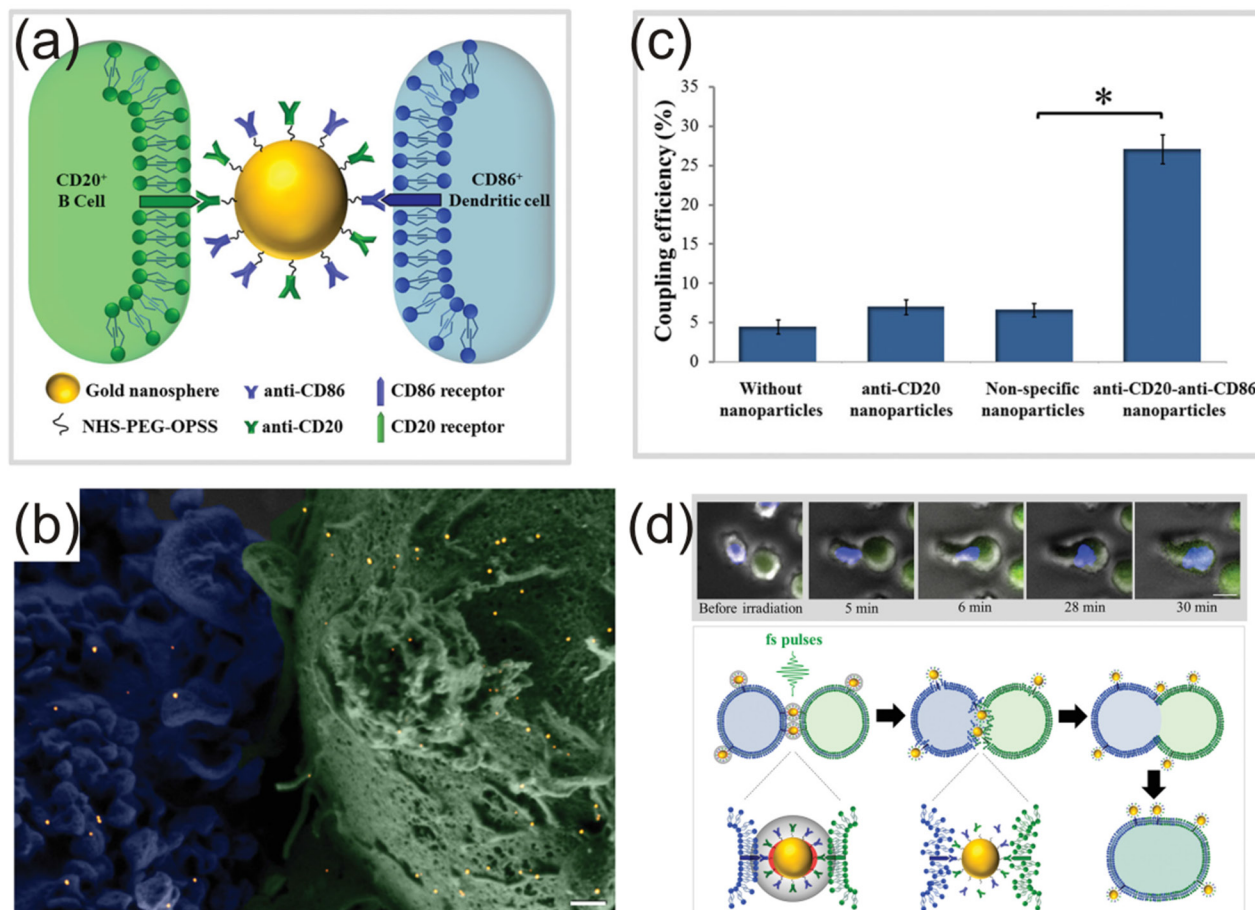


**Figure 9.** Coupling and fusion of cells using irradiation of bispecific conjugated GNPs linking a DC cell with a BJAB cell. (a) Details of the coupling strategy using two different antibodies coupled to a single GNP. The antibodies (anti-CD86 and anti-CD20) bind to the respective receptors expressed by DC and malignant BJAB cells, respectively. (b) A high magnification scanning electron microscopy (SEM) image of a DC (blue) coupled to a BJAB cell (green). GNPs are shown in yellow. The ruffled cell surfaces clearly indicate that cells need tight adhesion for successful fusion to happen. Scale bar, 200 nm. (c) Coupling efficiency for cells in presence or absence of GNPs. GNPs conjugated with monospecific antibodies (anti-CD20) have nearly no effect on coupling efficiency. However, conjugation of anti-CD20 and anti-CD86 on the same GNP raises the coupling efficiency from ~6% to ~26%. (d) Images of a fusion event between a DC cell and a BJAB cell. After 30 min the blue nucleus of the DC cell (labeled with Hoechst) is well encapsulated within the BJAB cell. The schematic below illustrates the individual steps and tentative mechanism behind the fusion. A mechanical shock wave from the fs pulse hitting the GNPs is thought to disrupt the adjacent membranes and lead to fusion. [65] John Wiley & Sons. Copyright © 2013 WILEY-VCH Verlag GmbH & Co. KGaA, Weinheim.

a micrometer sized focus and the particles could be additionally heated at higher laser powers.

GNPs trapped in three dimensions have also been found to heat significantly in a NIR optical trap. By trapping GNPs near gel phase GUVs, which had well defined melting transitions and served as thermal sensors, it was found that GNPs with sizes between 80 and 200 nm reached temperatures up to ~180 °C when trapped with  $P = 600$  mW at the focal region [68]. In other studies the temperature dependent viscosity of water and its effect on Brownian motion have been used to infer the surface temperature of GNPs or gold nanorods (GNRs) which were optically trapped using NIR lasers [69, 70]. In these studies optically trapped GNPs had a heating rate of  $266 \text{ K W}^{-1}$  [69] and GNRs were found to heat with a rate of  $900 \text{ K W}^{-1}$  [70]. We conclude that optical trapping of metallic nanostructures using NIR lasers produces sufficient local heating for causing severe, but highly localized thermal stress on biological material and hence has the potential to facilitate membrane fusion.

**3.1.3. Optical trapping of metal nanoparticles.** As mentioned in the previous section several studies have reported 3D optical trapping of different types of nanoparticles. Stable optical trapping of metallic nanoparticles requires that the particles have a high polarizability and that the radiation pressure, which scales with the extinction cross section, is not too large. These requirements are valid for most metallic nanoparticles tested so far. Several nanoparticles with different shapes, material, sizes etc, have been optically trapped in three dimensions and we provide a selection of studies in the overview given in table 1. The table also includes associated heating in the cases where the heating was quantified. The optically trapped spherical nanoparticles were smaller than 250 nm in diameter and the smallest nanoparticles to be trapped by a conventional NIR optical trap had diameters of ca. 5–10 nm [71, 72]. Gold nanoshells and GNRs provide new interesting possibilities since these can be trapped and also can be designed to have tunable resonances across the visible spectrum to the NIR

spectrum simply by changing the core/shell ratio (for shells) or the width/length ratio (for rods) [73].

The theoretical description of optical trapping is derived from the energy of a dipole in a gradient optical field. The nanoparticle is considered as a dipole which becomes polarized by the field and both absorbs and scatters the incoming light. The gradient force on a dipole in an electromagnetic field  $E$  is given by

$$\mathbf{F} = \frac{1}{2} |\alpha| \nabla \langle \mathbf{E}^2 \rangle. \quad (2)$$

Hence, the force points along the gradient of the intensity which is always towards the center of a focused beam where the intensity is highest. The shape of the intensity distribution is clearly an important parameter in determining the optical forces on a particle. Notably, it has been shown that, due to spherical aberration, a focused laser beam has a complex 3D intensity distribution with intensity maximum at the focus, but with additional local maxima in the vicinity of the focus [79]. This makes it inherently difficult to predict the trapping position, the optical forces and the optical heating on optically trapped nanoparticles [68, 79]. It is therefore imperative to rely on actual temperature measurements of trapped nanoparticles, rather than on theoretical calculations alone, to assess the heating under any given experimental conditions.

Metallic nanoparticles have relatively high extinction cross sections and hence experience significant radiation pressure in an optical trap [84]. The radiation force scales linearly with the extinction cross section and is given by

$$\mathbf{F}_{\text{rad}} = \frac{n \langle \mathbf{P} \rangle}{c} C_{\text{ext}}, \quad (3)$$

where  $\langle \mathbf{P} \rangle$  is the time averaged Poynting vector,  $c$  is the speed of light, and  $n$  is the index of refraction. Stable trapping is achieved when the gradient force in equation (2) exceeds the radiation force given in equation (3), in the direction along the beam. The radiation force on optically trapped 80 nm GNPs was recently quantified in [75].

We conclude that NIR optical trapping and heating of nanoparticles is versatile tool for achieving nanoscale control of heating. With the large diversity of accessible nanomaterials and nanostructures exhibiting vastly different optical properties, this approach must be considered rather unexplored in particular with regard to the use of optically controlled nanoheaters for manipulating living cells and soft matter systems. In the following sections, we present some recent developments demonstrating the potential of this system for fusing synthetic membranes, native plasma membranes and living cells.

### 3.2. Fusion between synthetic vesicles (GUV–GUV fusion)

In [4], a highly selective and efficient physical method was introduced to trigger membrane fusion between two GUVs. This flexible method, illustrated in figure 11, can trigger membrane fusion between synthetic vesicles of different membrane charge, different physical state (gel/fluid), and different size (10–200  $\mu\text{m}$  in diameter) as shown in [4]. Complete lipid mixing

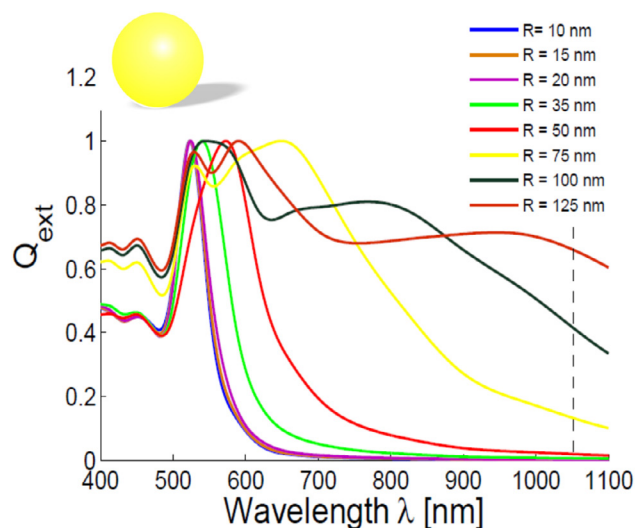


**Figure 10.** Normalized extinction cross section of spherical GNPs with radii from 10 nm to 125 nm. The spectra are calculated using Mie's equations. A frequently used wavelength for optical trapping of GNPs is 1064 nm which is marked by a vertical dashed line. Reproduced with permission from [95]. © Copyright 2014 IEEE - All rights reserved.

(figures 11(a)–(c)) and content mixing (figures 11(d)–(f)) were verified and thus, the technique can be used to study induced chemical reactions within picoliter volumes.

GUVs are spherical lipid bilayers of microscopic dimensions which are formed from the closure of an already existing lipid bilayer to a curved vesicle [97]. Standard electroformation is the most common method to synthesize GUVs in a highly efficient manner. Electroformation relies on employing AC fields to form vesicles from a dried film of lipids deposited onto a conductive surface while the film is being hydrated. It has been proposed that the external electrical field during hydration induces lipid swelling and vesicle formation by facilitating bilayer separation and bending which are two important prerequisites for vesicle formation [98].

Fusing two GUVs requires expansion of the lipid bilayers at their contact area thereby leading to a transient opening in the two opposing membranes and formation of a fusion pore. This process is associated with a high energy barrier and will not occur spontaneously [1].

The fusion method presented in figure 11 is based on using optical tweezers (1064 nm NIR laser) to select two GUVs of interest and bring them into immediate contact. The same NIR laser focus is then positioned at the contact zone of the two GUVs until a GNP diffuses from the surrounding buffer into the laser focus. The trapped GNP absorbs NIR light which becomes converted into heat that dissipates locally. One important advantage of this method is the fact that the length scale of the plasmonic heating is comparable to the diameter of the GNP [35]. The temperature elevation can expand the area of fluid phase lipid bilayers by  $\sim 0.5\%$  per degree [99] and the area of gel phase lipid bilayers by  $\sim 20\text{--}25\%$  (if the temperature is ramped up across their phase transition temperature) [100]. Consequently, the GNP has to be positioned at the exact spot where the membranes make contact and it should be irradiated with sufficiently high laser power to generate

**Table 1.** Overview of some common metallic nanostructures which can be optically heated and trapped in three dimensions using a focused CW laser beam. The table provides references to respective studies in which different particles were optically trapped or heating was quantified.

Particle type	Size	Trapping	Heating
Gold nanoparticles	10–250 nm	[23, 34, 68, 71, 72, 74–81]	[35, 68, 69, 78, 82–84]
Silver nanoparticles	20–275 nm	[85–89]	[88] <sup>a</sup>
Gold nanorods	Diameter down to 8 nm	[70, 90–92]	[70, 93, 94]
Gold nanoshells	150 nm	[95, 96]	[82]

<sup>a</sup> The temperatures of trapped Ag monomers and dimers were simulated.

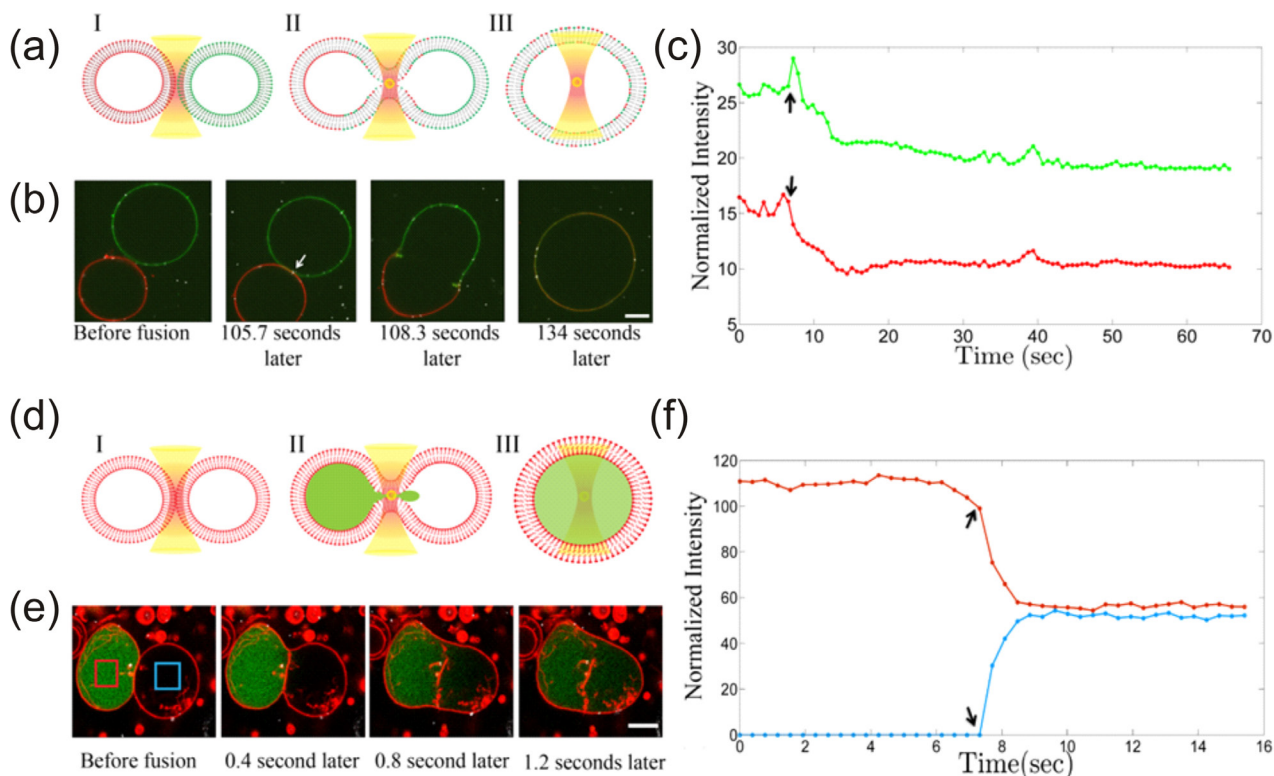


**Figure 11.** Complete Vesicle fusion triggered by optically heated GNPs. Cartoons in (a) and (d) depict lipid mixing and content mixing while membrane fusion is triggered by means of laser-induced heating of a GNP. (b) and (e) Are confocal image series showing the same stages as illustrated in (a) and (d), respectively. A white arrow in (b) is used to point out a 80 nm GNP, seen as a bright spot in the contact zone of the two GUVs. The scale bar is 10  $\mu\text{m}$  in both image series. The plot shown in (c) corresponds to the experiment illustrated in (b); the normalized emitted intensities from Fast-DiO (green) and Texas-red (red) are plotted as a function of time. Black arrows show the fusion pore opening upon which both intensities drop quickly because of lipid mixing. (f) Cargo mixing corresponding to the experiment shown in (e). The intensity of the green hydrophilic fluorophore, calcein, is normalized per pixel and plotted as a function of time; the red trace and blue trace in this plot are from the red and blue boxes shown in (e). Black arrows show the moment of fusion pore opening after which calcein intensity uniformly distributes inside the fused GUV within a few seconds. Lipid composition of GUVs: 10% DOPS, 90% DOPC in (b) and 20% DOPS, 90% DOPC in (e) with trace amounts of membrane dyes. In both (b) and (e) 80 nm GNPs were trapped using a laser power at the samples of 200 mW. Reprinted with permission from [4]. Copyright (2015) American Chemical Society.

a nanometric disruption in the adjacent lipid bilayers. The disruption is then followed by a rearrangement of the lipid bilayers into one fused structure. Complete lipid and content mixing verify the merging of the vesicles into one fully fused vesicle.

Stable trapping of GUVs by optical tweezers is feasible if the GUV's lumen has a higher refractive index with respect to the surrounding buffer. By encapsulation of sucrose solutions within GUVs during electroformation, the index of refraction can be increased sufficiently to allow trapping [4, 21]. To efficiently trigger fusion by this method, it was found that the membrane tension should be minimized as it can make it

more difficult for the two fusing GUVs to be in sufficiently close contact. To achieve this it is recommendable: (1) to use a hypertonic buffer outside the GUVs and: (2) to use an appropriate coating on the surface to minimize the adhesion induced increase in membrane tension.

**3.2.1. Content and lipid mixing.** Observation of lipid mixing, content mixing or measuring the size of the fused vesicle are three commonly used approaches for verifying membrane fusion [4]. For instance, confocal imaging can be used to validate fusion by lipid and content mixing within the two fusing vesicles. In figure 11(b), the membranes of the two GUVs are

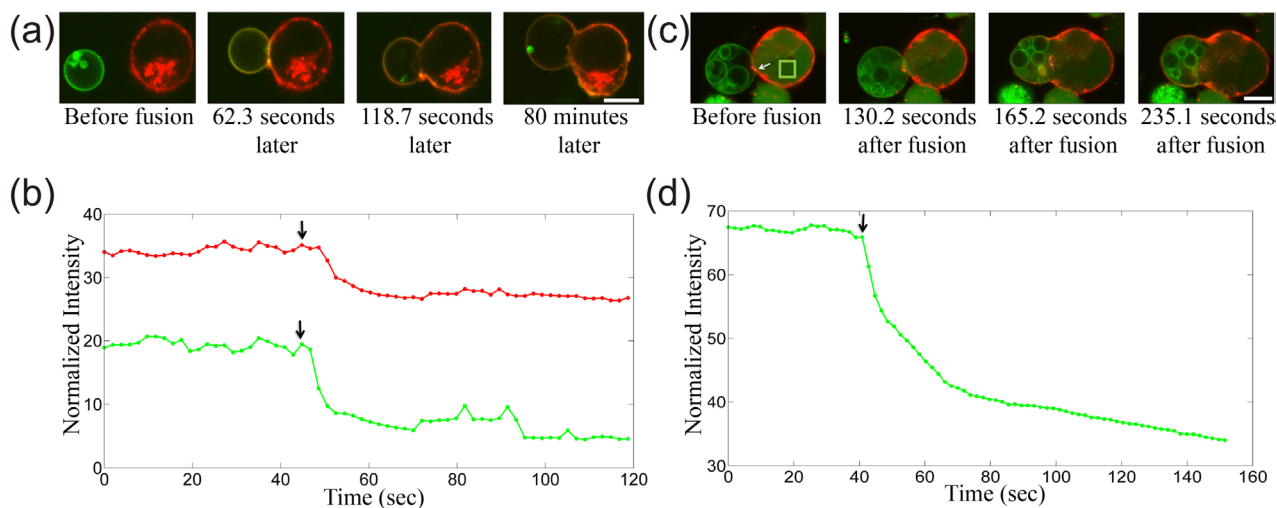


**Figure 12.** Lipid mixing and lumen mixing associated with heat induced fusion of GUVs to living HEK293 cells. (a) and (c) are time series of confocal images of lipid mixing and lumen mixing, respectively. The GNP is visible as a bright spot (reflection signal) in (c) (white arrow). Scale bars are  $10\ \mu\text{m}$ . The plot in (b) shows the time evolution of intensity from Fast-DiO (green) and vybrant<sup>®</sup> DiD (red) for the experiment shown in (a). (d) Fusion and associated lumen mixing verified by quantifying the intensity of calcein within the green box, shown in (c), over time. The black arrows in (b) and (d) show the time when lipids and lumens start to mix due to formation of the fusion pore. Additional examples are provided in [22]. The lipid composition used in both (a) and (c): DOPC 98.5 mol.%, biot-DSPE-PEG 1 mol.%, FAST-DiO 0.5 mol.% Laser power at the sample for (a) and (c): 400 mW and 450 mW respectively. GNP size for both (a) and (c): 80 nm. [22] (2017) © Tsinghua University Press and Springer-Verlag Berlin Heidelberg 2016. With permission of Springer.

labeled by two different lipophilic fluorophores and are imaged by a confocal microscope. As shown in figure 11(c), the two lipophilic fluorophores undergo a simultaneous dilution upon fusion because they possess a conserved number of fluorophores which are distributed over a larger area of the membrane after fusion. The time scale for lipid mixing depends on the physical state and the size of GUVs. For fluid phase vesicles the time scale for mixing is  $\sim 10\text{s}$  as shown in figure 11(b, c). When a gel phase GUV fuses to a fluid phase GUV the time scale of mixing is significantly longer which is also shown in [4]. This is expected as the mobility of lipids is significantly lower in gel phase membranes compared to their mobility in fluid phase membranes. The experimentally obtained time scales for lipid mixing are found to be reasonably close to the time scales obtained from a quantitative model which describes the lateral diffusion in spherical shells [4, 101]. Therefore, it can be concluded that the lipid mixing following fusion is governed by diffusion of molecules within the 2D membrane.

Content mixing can be validated by fusing a GUV filled with calcein (green lumen in figure 11(e)) to an empty GUV (black lumen in figure 11(e)) and by tracking the changes in the intensity of calcein as a function of time (see figures 11(e) and (f)). Upon fusion, calcein diffuses from the calcein containing GUV to the calcein free GUV and eventually it becomes uniformly distributed within the larger volume after fusion. An example of quantification of cargo mixing is shown in figure 11(f). The time scale for content mixing depends on the size of the GUVs, but due to the much larger diffusion constant of calcein in aqueous solution ( $333\ \mu\text{m}^2\ \text{s}^{-1}$ ) [102] than lipid dyes in 2D membranes ( $10\text{--}15\ \mu\text{m}^2\ \text{s}^{-1}$ ), content mixing occurs at least one order of magnitude faster than lipid mixing.

If the method presented in figure 11 should be extended to smaller nanoscale lipid vesicle systems it would probably

necessitate the use of smaller GNPs to minimize the distance between nanoscale vesicles to be fused. The smallest GNPs used so far in GUV–GUV fusion have been 80 nm GNPs which produce significant heat when trapped at  $\sim 200\ \text{mW}$  of laser power. Since the absorption cross section of nanoparticles scales with volume the smaller nanoparticles will tend to heat much less and are unlikely to produce sufficient heat for fusion. However, it should be noted that certain nanostructures, like titanium and platinum nanoparticles, have higher absorption cross sections than gold in the NIR region and could allow for fusion with smaller nanoparticle sizes.

### 3.3. Cell-GUV fusion

The hot-nanoparticle mediated membrane fusion method introduced in [4] utilizes a NIR laser for trapping the GNP. While extending the method to living cells it is important to ensure that both the laser light and the localized heating do not compromise the viability of the cells.

Successful fusion of a GUVs to a living cell using the hot-nanoparticle mediated fusion method was reported in [22]. Optical control was utilized to fuse a selected GUV to an individual HEK293 cell. Such experiments are of particular importance as they can be potentially used for different biomedical applications including targeted drug delivery at the single cell level, delivering new lipids/new proteins to the membrane of the live cell of choice and for transferring small regulatory RNA molecules to a selected cell to control gene expression. It is important to minimize the plasmonic heating sufficiently to avoid the risk of heat induced damage on the live cell during fusion. This is done by using smaller GNPs, by using the lowest laser power necessary for cell fusion, and by minimizing GNP aggregation. To verify full fusion between a cell and a GUV the intensity and distribution of lipophilic membrane

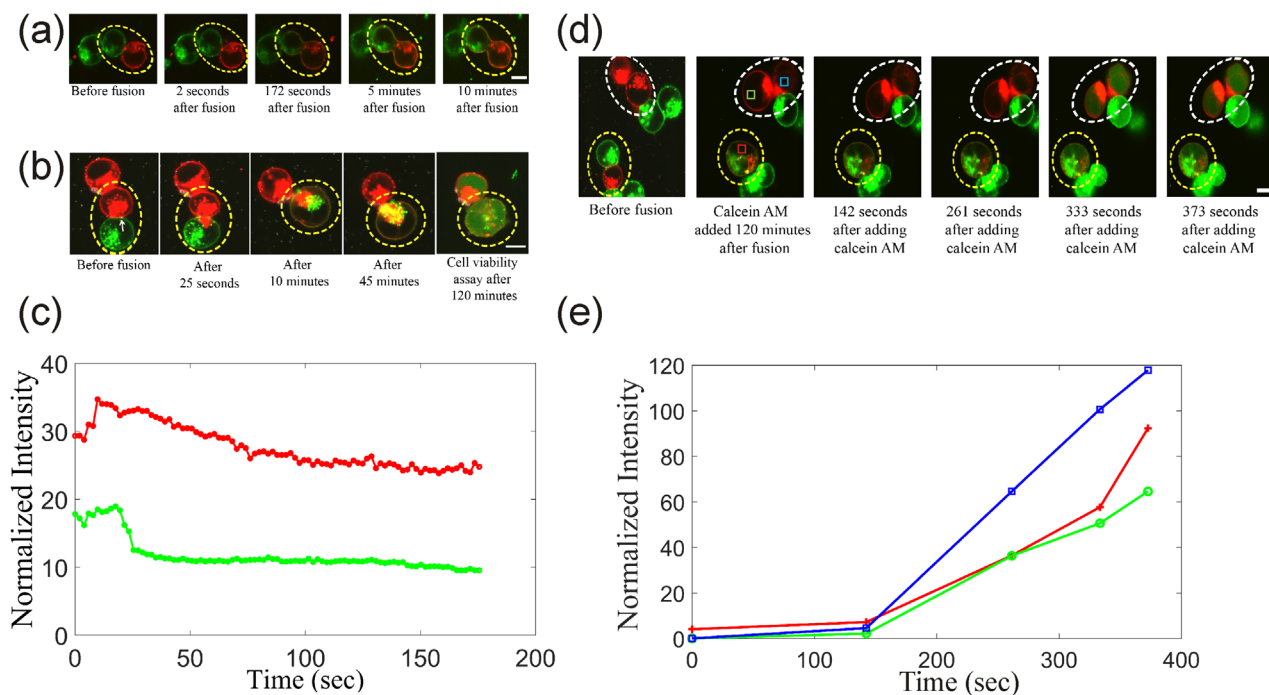


**Figure 13.** Optically controlled fusion and associated mixing of the plasma membranes and cytoplasmic mixing. (a), (b) and (d) Confocal image series of three examples of fusions of HEK293 cells, labeled by vybrant<sup>®</sup> DiD (red), and by vybrant<sup>®</sup> DiO (green), respectively. The two fusing cells are surrounded by a dashed yellow ellipse. Scale bar in all image series is 10  $\mu\text{m}$ . The GNP in the contact zone of the adjacent membranes is pointed out by using a white arrow in (b). The plot in (c) represents the time evolution of intensity per area for the two lipophilic fluorophores. Fusion occurs at  $t \sim 20$  s and is followed by a reduction of the intensity of both fluorophores. (d) Investigation of the invasiveness of the hot GNP induced fusion for live cells. The two HEK293 cells surrounded by the yellow dashed ellipse are remotely fused by means of optically controlled heating. Calcein AM was injected to the sample chamber 2 h after fusion to investigate their viability. The green intensity indicates enzymatic activity and the membrane integrity of the cells. (e) Normalized green intensity emitted by calcein in the formed syncytium (the blue line) and the two control cells surrounded by the dashed white ellipse in (d) (the red and the orange lines). Data points in each line correspond to the intensity of calcein in the images shown in (d) (2nd–5th image). The level of emitted green color in the syncytium is comparable to the control cells. 150 nm GNPs were used for fusing the cells and the laser powers were (a) 450 mW, (b) and (d) 250 mW at the sample. [22] (2017) © Tsinghua University Press and Springer-Verlag Berlin Heidelberg 2016. With permission of Springer.

markers and hydrophilic lumen markers can be monitored, as was done in [22]. Examples from two such experiments are shown in figures 12(a) and (b). Here, the fusing GUVs contain sucrose and are labeled with the lipid analog, Fast-DiO (green). Successful fusion was achieved by first conjugating GNPs to the GUVs through biotin-streptavidin linkages. The mobility of the GNPs on the fluid membrane ensured that a GNP could be optically trapped at the contact area between the GUV and the cell. The GUVs were suspended in a slightly hypertonic imaging medium containing HEK293 cells. In figure 12(b), the time evolution of intensities of Fast-DiO (GUV membrane) and vybrant<sup>®</sup> DiD (cell membrane) are normalized per pixel and plotted. The sudden change in both intensities clearly indicates the onset of lipid mixing between the cell and the GUV. The intensity decrease is more pronounced for FAST-DiO than that of vybrant<sup>®</sup> DiD because the area of the GUV membrane is smaller than the cell membrane. Lumen mixing in cell-GUV fusion was also verified in [22] by labeling the cell lumen with calcein, see also the example in figures 12(c) and (d). The diffusion of green calcein from the cytoplasm into the lumen of the GUV clearly indicates formation of a fusion pore. However, despite there is no membrane barrier between the cell and the GUV after fusion, cytoplasmic crowding by cytoskeletal structures and cell organelles slow down

the time scale of lumen mixing for cell-GUV compared to that of GUV-GUV fusion [4, 103].

Viability of cells following fusion to a GUV is likely to be compromised by the large volume of sucrose added to the cytoplasm upon fusion [22]. Long term viability studies need to be performed, but the fusion experiments most likely have to be optimized with regard to making the internal GUV composition resemble more the physiological environment of the cell and preferentially by using smaller GUVs to minimize the change in the composition of the cytoplasm of the fused cell.

### 3.4. Cell-cell fusion

The fusion method presented in figure 11 was shown to be applicable for fusing two cells if slightly larger GNPs were used [22]. This approach thus offers a unique strategy for remote fusion of selected cells in a random population of cells.

Figure 13 shows a realization of fusion of two fluorescently labeled HEK293 cells, one labeled green and the other red. The process is imaged by a confocal microscope with clear evidence of full fusion as verified by both mixing of the plasma membrane (figures 13(a) and (c)), and mixing of the internal membrane structures (figures 13(b) and (c)). Upon fusion a drastic decrease is seen in the intensity of both

vybrant® DiD (the red fluorophore) and vybrant® DiO (the green fluorophore) as they redistribute within a larger membrane area. The lipid mixing time scale is slower in cell–cell fusion experiments compared to mixing in model membranes. This is probably caused by a frictional coupling to the protein crowded membrane environment and by physical interactions between lipids and the cell's cytoskeleton. The two cells eventually merge into one spherical structure containing the cytoplasm and organelles from two cells. The mixing of the two cytoplasms can be seen in figure 13(b) where the yellow color appears as a result of complete mixing of green and red membrane surrounded organelles of the two original HEK293 cells. It takes ~45 min for this complete cytoplasmic mixing to occur.

The fused cells are found to be viable as shown in the calcein AM assay as shown in figures 13(b), (d) and (e), thus suggesting that the syncytium is viable immediately after fusion. In [22] metabolic activity in the fused cells was also reported for up to 4 h following fusion.

Membrane integrity and esterase activity is a sign of cell viability. In the calcein AM viability test, the enzymatically induced green fluorescing molecules can only be trapped in the cytoplasm of the cell if the integrity of its plasma membrane is not compromised. Beside the esterase activity and plasma membrane integrity, which were tested by the calcein AM assay, the metabolic activity of a fused syncytium was also tested in [22] by using a tetrazolium (MTT 3-(4,5-dimethylthiazol-2-yl)-2,5-diphenyltetrazolium bromide) assay [104, 105] performed on single cells. The tested syncytia were found to exhibit metabolic activity 4 h after fusion. However, further experiments are needed to verify long-term viability, to test whether nuclear fusion is feasible, and whether the novel hybrid cell undergoes cell division.

#### 4. Applications of optically mediated membrane fusion

The use of electromagnetic field induced fusion of cells and membrane vesicles offers new opportunities for researchers to manipulate the content of single cells and vesicles. In particular genetic manipulation of cells becomes feasible with introduction of plasmids into the cytoplasm of selected cells or mixing of the genomes of different cells. Also, pico-liter chemistry is a direct consequence of fusion of GUVs containing either chemical reactants or biologically active molecules and the reactions can then be studied in real time under a fluorescent microscope. In the following sections we review some of these recent advancements which clearly demonstrate the potential in applying remotely controlled membrane fusion for studying membrane protein dynamics and for manipulating cells.

##### 4.1. Triggering protein binding by controlling membrane composition

Membrane lipid compositions critically affect protein bindings to membranes and hence are decisive for how membranes

are regulated by proteins. A class of membrane shaping proteins containing BAR (Bin-Amphiphysin-Rvs) domains bind to acidic membranes in a charge dependent manner and these proteins are therefore highly sensitive to the density of negatively charged lipids in the membrane [106]. BAR domains collectively shape flat membranes into tubes or vesicles by imposing their molecular bent shape on the softer membrane [106]. Studies of the binding kinetics and membrane curvature effects induced by BAR domain proteins are mostly performed on GUVs by adding the protein to the exterior solution. However, most BAR containing proteins have their natural location in the cytoplasm and therefore, in a more biologically relevant model experiment, the protein should be encapsulated inside GUVs. Encapsulation of BAR domains inside GUVs composed of negatively charged lipids is difficult due to the binding of the protein to the lipids during formation of the GUVs [38]. However, fusion of GUVs offers a straight forward solution to this problem since proteins can be encapsulated within neutrally charged GUVs and subsequently be fused to highly negatively charged GUVs, thus enabling protein binding to the membrane.

This strategy was employed in [4] where protein binding was activated by changing the lipid composition via fusion of two GUVs using the hot-nanoparticle-method, see figure 14. First, IM (IRSp53/MIM homology) domains (termed I-BAR domains) from the protein ABBA were encapsulated within GUVs composed of DOPC lipids. These lipids are zwitterionic and hence I-BAR cannot bind electrostatically to the membrane of such vesicles neither during GUV formation nor later after their formation. After fusion of these neutral GUVs to negatively charged GUVs, membrane binding of I-BAR was activated with consequent outwards tubulation of the membrane, see figure 14(b). These observations are supported by the biological role of I-BARs in cells where the protein is found to be enriched inside tubular protrusion in cells called filopodia.

The experiments presented in figure 14 can be used for studying the membrane shaping ability of other BAR domains (N-BAR, pink-BAR or F-BAR) which have different molecular shape and hence will deform the membrane into a different morphology such as inwards tubulation or possibly spherical buddings. Another interesting exploration of this assay would be to do biological chemistry within the lumen of the GUVs; by encapsulating polymerization buffer within one GUV and monomers in a second GUV it should be feasible to trigger polymerization of structures like F-actin or microtubules within GUVs and monitor the process.

##### 4.2. Fusion of GPMVs to artificial membrane vesicles

Artificial membranes are often used to study proteins as shown in the previous section. However, native membranes exhibit a great diversity of lipid species and transmembrane and anchored proteins occupy a considerable fraction (ca. 50%) of the surface area of cells. Efforts have been made to reconstitute transmembrane proteins in artificial membranes, but such experiments are difficult and suffer from lack of control over protein orientation in the membrane. Moreover,

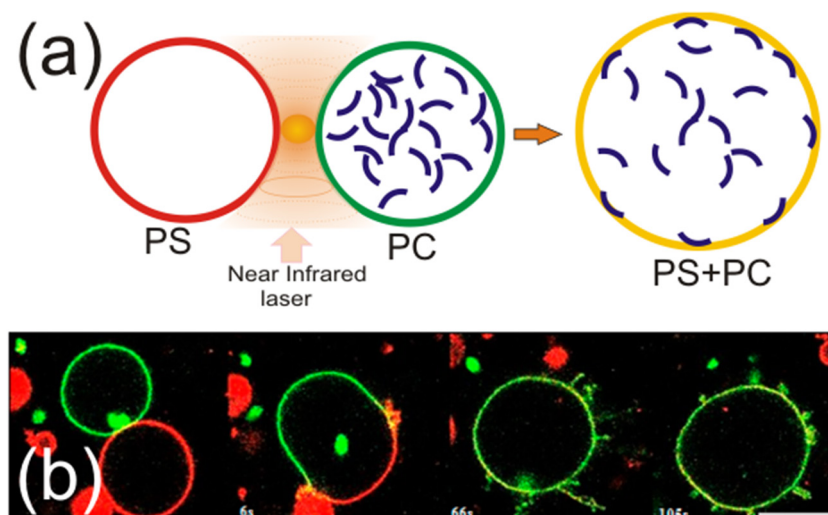


**Figure 14.** Hot-nanoparticle-mediated membrane fusion used in biophysical experiments with membrane binding proteins. (a) Schematic depiction of the experiment. IM (IRSp53/MIM homology) domains from the protein ABBA are encapsulated within GUVs made from neutral lipids. Upon fusion with GUVs made from acidic lipids, protein binding is switched ‘on’. (b) Confocal images of the fusion experiment depicted in (a). The GUVs are made from pure DOPC (green GUVs) or contain a mixture of 40% of DOPS and 60% DOPC lipids (red GUVs) and are labeled red and green using trace amounts of Texas Red conjugated lipids and FAST-DiO, respectively. After fusion the lipid dyes mix within seconds and the membrane binding of I-BAR leads to outwards tubulation (last image to the right) due to the membrane shaping ability of I-BAR. Reprinted with permission from [4]. Copyright (2015) American Chemical Society.

the complex protein environment and factors like crowding [107, 108] in a native cell membrane can contribute to the function of a single type of protein.

To study proteins in their native membrane, but in absence of internal cell structures like the nucleus and cytoskeleton, a technique has been developed to extract the cell membrane from cells to form so-called GPMVs. These membranes contain the rich natural content of membrane proteins, as present in plasma membranes, and additionally contain the aqueous cytosol from the cell interior. Even though GPMV membranes are chemically derived, their composition and behavior resembles the native cellular plasma membrane, but with no underlying cytoskeleton [109].

Optically induced fusion offers the exciting possibility to combine both native and synthetic lipid bilayers for studying how the change of lipid composition affects motility of proteins, or for performing controlled picoliter biochemistry by mixing of reactants contained in separated GUVs with cytosol from the GPMVs. We show here how the fusion of artificial bilayers (GUVs) and native plasma membrane (GPMVs) can be successfully carried out using the same fusion method as reported in [4].

GPMVs were formed by a published procedure from [110]. Chemically induced GPMV’s from HEK293T cells detached from the cell body and could be harvested for further experiments. GPMVs were membrane labeled by adding vibrant DiD solution to the cells prior to bleb formation and the content of the GUV was detected using encapsulated calcein.

Fusion of GPMVs to GUVs occurred when a GNP with  $d = 80\text{ nm}$  diffused into the optical trap which was located at the contact area between the vesicles. Non-leaky content and lipid mixing was observed for the fusion between the GUVs and GPMVs, see figure 15(b). The content and lipid dyes mixed within seconds as quantified in figure 15(c) with the

content mixing being  $\sim 20$  times faster. The mixing of lipids was noticeably much faster during GPMV fusion, as shown in figure 15, compared to when a GUV was fused to a living cell. This indicates that the membrane of a cell exhibits significant friction with the cortical cytoskeleton.

The results in figure 15 clearly show that GPMVs are a great tool for studying membrane proteins in applications where the membrane compositions can be altered by fusion with GUVs with a known composition. Additionally, picoliter biological biochemistry inside the GPMVs can be explored by fusing GUVs, containing actin or microtubule monomers, to GPMVs containing all the necessary components for polymerization, bundling protein and linker proteins for linking cytoskeletal polymers to the membrane.

#### 4.3. Transfer of bio- and inorganic materials between cells and vesicles

Transfer of biomaterials or beads into the cytoplasm of living cells is a common procedure in biological and biophysical research. Transient transfection of cells is usually performed by complexing DNA with cationic molecules which are taken up by cells when added to a cell culture. Transfection of single cells can be achieved by fusion of GUVs containing the relevant plasmid for transfection. In [10] electrofusion was used to transfer both plasmid and microbeads into the intracellular environment of HeLa cells, see figure 16(a). Encapsulation of beads and plasmid was done using standard emulsion techniques for GUV formation. By applying an AC electric field the cell and GUV were aligned and a subsequent DC pulse fused the structures and delivery of the beads and plasmid could be detected inside the fused cell, see figure 16(b). Successful transfection was confirmed by expression of

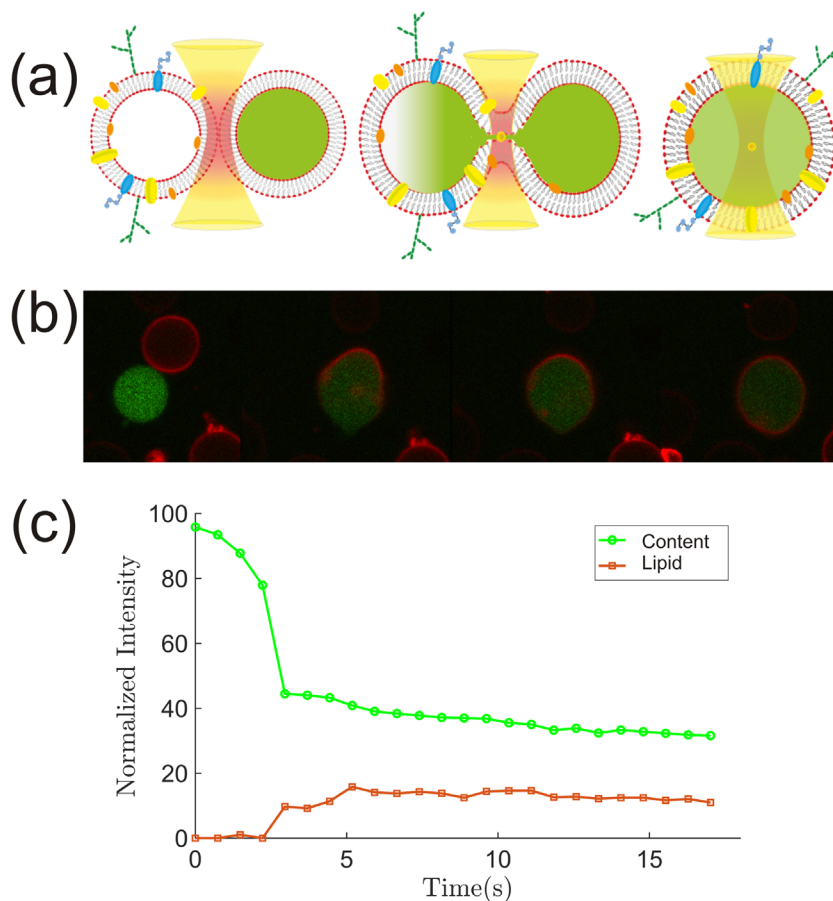


**Figure 15.** Hot-nanoparticle-mediated fusion of GUVs with cell extracted GPMVs. (a) Schematic depiction of the fusion between a GUV and a GPMV by optical trapping of a 80 nm GNP at the contact area between the membrane vesicles. The GPMV membrane was labeled with vybrant DiD to monitor lipid mixing and the interior of the GUV was loaded with calcein for monitoring content mixing. Confocal images showing fusion between a GUV (green lumen) and a GPMV (red membrane). (c) Time evolution of the intensities shows that both lumen and membrane mixing occur within seconds. Unpublished results.

fluorescent mCherry encoded by the plasmid (red color in figure 16(b)). These experiments clearly show that fusion of GUVs can be used to genetically modify single cells and also for transfer of larger particles which are typically delivered by potentially invasive and advanced micropipette injection.

In a recent study [111] delivery of nanoparticles to the cytoplasm of cells was triggered by illuminating pH sensitive liposomes, containing nanoparticles, using UV light. A drop in pH upon irradiation destabilized the liposome membrane and triggered fusion to the MDCK cells and delivery of nanoparticles to the cytoplasm. Optical manipulation was performed on these nanoparticles within the cytoplasm and they served as intracellular fluorescent temperature sensors.

Fusion of GUVs has interesting applications in inorganic picoliter chemistry. Different GUVs can readily be loaded with small soluble reactants which form a fluorescent product upon mixing. This strategy was followed by Yang *et al* [36] to synthesize fluorescent quantum dots (QDs) from the two chemicals,  $\text{CdCl}_2$  and  $\text{Na}_2\text{S}$ , which were encapsulated within two fluorescently labeled GUVs as shown in figure 16(c). The diameters of the QDs were measured by transmission electron microscopy (TEM) to be 4–8 nm. The stability of the nanoparticle product was not reported and the imaging of single QDs fluorescent emission was not performed.

## 5. Discussion

Electrofusion and fusion mediated by lasers have been used to fuse a number of different cell types and membrane vesicles. In most studies, fusion is reported for one or two cell types using a single technique. While most studies include viability tests of the fused hybrid cells, no standard viability test or viability criteria have been used which makes comparison between techniques difficult. Additionally, fusion efficiencies of the respective methods are hard to compare since the different strategies used for cell pairing strongly affect the success rate of fusion.

In table 2 we provide an overview of some cell types which have been fused using electrofusion, pulsed lasers, or the hot-nanoparticle-mediated fusion method presented in section 3. The overview includes several methods for cell pairing, the reported fusion efficiency, and how long the viability of the cells was monitored. Studies reporting fusion between GUVs or between GUVs and cells are also included in the table 2.

From table 2 it can be concluded that fusion can be achieved for a number of cell types using different techniques and fusion efficiencies generally lie within the range 10–90%. The highest fusion efficiencies are obtained if proper cell pairing is achieved using, e.g., a microfluidic device containing microstructured cell traps.

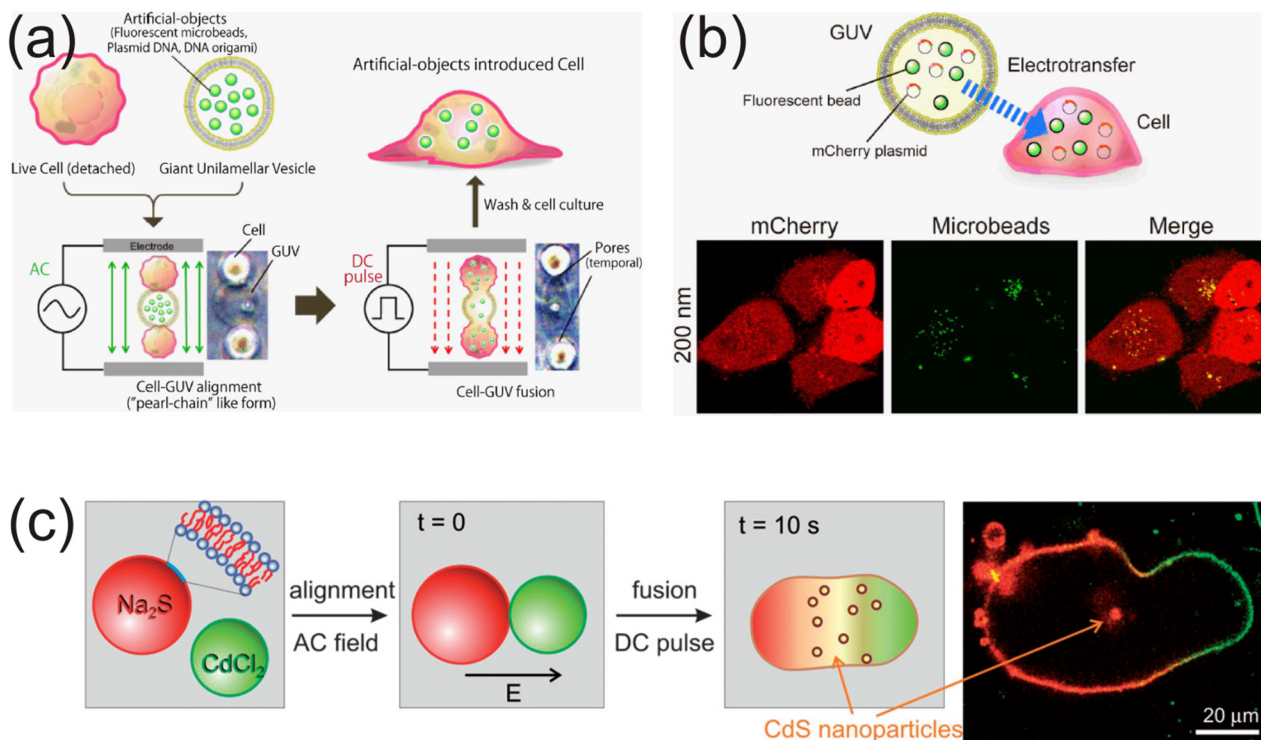


**Figure 16.** Applications of electrofusion in cell delivery and for pico-liter chemistry. (a) Schematic illustration of the electrofusion protocol for fusing a GUV to cells. GUVs, containing beads, DNA plasmids or DNA origamis, are first aligned by using an AC electric field and subsequent application of a DC pulse triggers fusion between a GUV and one or two cells. (b) Transfer of biomaterial or beads into the cytoplasm of cells by using the electrotransfer technique. Fluorescent images show micron sized beads (green) and the homogenous distribution of mCherry (red) which is encoded by the transferred plasmid. (c) Application of GUV electrofusion to synthesis of quantum dot nanoparticles (QDs) by mixing of two chemical reactants.  $\text{Na}_2\text{S}$  encapsulated in the first GUV, was mixed with  $\text{CdCl}_2$  encapsulated in a second GUV by application of an electric pulse. The last image is a confocal snapshot of the fusion process resulting from a red-labeled GUV (containing  $\text{Na}_2\text{S}$ ) fused to a green-labeled GUV (containing  $\text{CdCl}_2$ ). The fluorescent QD product forms after a few seconds and is marked by an arrow in the confocal image. Panels (a) and (b) Reproduced from [10]. CC BY 3.0. Panels (c) and (d), [36] John Wiley & Sons. Copyright © 2009 Wiley-VCH Verlag GmbH & Co. KGaA, Weinheim.

Cell viabilities can be tested using standard viability assays which can provide a fast viability check of the fused cell a few hours after fusion [115, 116]. However, a better validation of the viability is to culture cells for days to demonstrate the ability of cells to divide and create a progeny containing a new genome [33, 111]. This was demonstrated in [33] where somatic cells were fused to stem cells and reprogramming of the cells was demonstrated by culturing the fused cells for days. Viability has been tested in most studies after a few hours and in a few studies for several days, see table 2. Generally, the viability is high in these viability assays which shows that optically induced fusion is a valuable technique for studying hybrid cells. We note that table 2 does not provide a complete overview in particular with respect to electrofusion which has been extensively applied in cell research.

### 5.1. Mechanism of fusion

Successful fusion of two membranes proceeds through three steps (i) bringing two membranes into close proximity (distance of a few nanometers) to establish a contact area between the membranes, (ii) destabilization of the two apposing membranes, and (iii) spontaneous fusion of the disrupted membranes into a single structure.

The first step is achieved by cell or vesicle pairing using optical trapping, microfluidic traps, micropipettes, dielectrophoresis, or simply by relying on random contacts. The second step requires energy to destabilize the bilayer structures. This energy can be delivered by a high transmembrane voltage in electrofusion by application of a DC pulse which destabilizes the two apposing bilayers and make them susceptible for fusion. Once the bilayer breaks a fusion pore nucleates and expansion of such a pore can have a velocity of a  $5 \text{ cm s}^{-1}$  in fusing GUVs [37]. To resolve such fast dynamics a fast camera with sub-millisecond time resolution has to be used. This effectively precludes standard fluorescence imaging and has to be performed using transmitted light. The mechanism behind electrofusion of Jurkat cells with GUVs was theoretically analyzed in [112] by using finite element modeling (FEM) to calculate the electric field. The calculations showed that a steady membrane potential was induced at the contact region between the cell and the GUV. Application of a pulsed electric field was predicted to result in a uniform membrane potential at the contact region after a few microseconds. These calculations were supported by experimental results showing that the fusion efficiency peaked at  $50 \mu\text{s}$ . Furthermore, this study found that fusion occurred by a uniform breakdown of the whole contact region which was rationalized by the FEM-predicted uniform membrane potential at the contact region.

**Table 2.** Overview of literature in which electrofusion and lasers have been employed for fusion of vesicles and cells. The table provides details of which cell types have been fused and the fusion efficiencies associated with various fusion methods. If a pairing method was used, then fusion efficiencies were measured for successfully paired cells only. Viability of the hybrid cells was measured in several studies after varying periods of time.

Cell/vesicle 1	Cell/vesicle 2	Method	Contact pairing	Eff.	Viable tested after	Ref.
HEK293	HEK293/GUV	OT/GNP <sub>150 nm</sub>	OT	—	4 h	[22]
HeLa	GUV	Electrofusion	Random	20%	5 d	[10]
MDCK	GUV	UV triggered pH induced fusion	OT	95%	—	[111]
COS 7	GUV	Electrofusion	OT/micropipette	20%	—	[48]
Jurkat	GUV	Electrofusion	Dielectrophoresis	22%	—	[112]
GUV	GUV	Optical trap/GNP <sub>80nm</sub>	OT	—	—	[4]
GUV	GUV	Electrofusion	Dielectrophoresis	—	—	[36, 37]
GUV	GUV	Electrofusion	Microstructure trap	—	—	[11]
GUV	GPMV	OT trap/GNP <sub>80 nm</sub>	OT	—	—	Unpublished
Macrophage/DC	BJAB-cell	FS laser GNP <sub>80 nm</sub>	Antigene coupling	7–20%	24 h	[65]
Myeloma (NS1)/3T3	Mouse B cell	Electrofusion	Microstructure trap	<89%	10 d	[33]
Mouse embryonic fibroblasts	Mouse embryonic stem cells	Electrofusion		<89%	10 d	[33]
HeLa	A549	Electrofusion	Microstructure trap	87%	24 h	[113]
MDA-MB-231	DC	Electrofusion	Random	30%	—	[42]
Myeloma (NS-1)	Myeloma (NS-1)	Ns laser	OT	11%	3 h	[12]
Chinese Hamster Ovary (CHO)	Mouse melanoma B16-F1	Electrofusion	Random/dielectrophoresis	<41%	24 h	[45, 47, 50]
Mesenchymal stem cells	Islet cells	Electrofusion	Dielectrophoresis	—	—	[44]
Human embryonic stem cells	Human embryonic stem cells	Ns Laser	OT	62%	12 h	[20]
B-cell lymphoma (BJAB)	Epidermoid carcinoma (A431)	Fs laser + GNP <sub>20 nm</sub>	Antigen coupling	—	23 h	[66]
Neuronal P19/Y79 retinoblastoma	Neuro 2A/Y79 retinoblastoma	Fs laser	OT	90%/95%	4 h	[52, 55, 17] <sup>a</sup>
HepG2	hESC	Ns laser	OT		48 h	[62]
PC-12	PC-12/NG 108–15/Jurkat/Cos 7	Electrofusion	OT/micropipette	<20%	20 h	[48]
Embryonic germ cells	Thymic lymphocytes	Electrofusion	Random	—	—	[9]
HepG2/HeLa	HeLa	Fs laser	OT	35–37%	4 h	[54]
B16-F1	CHO	Electrofusion	Random	<9%	15 min	[46]

<sup>a</sup> The cells were hemifused with merging of proximal leaflets only.

Abbreviations: Ns: nano-second, Fs: femto-second, OT: optical Tweezers, CHO: Chinese Hamster Ovary cells, HEK293: human embryonic kidney cells, PC-12: pheochromocytoma cells.

However, the experimental measurements were limited by a 33 ms time resolution for the imaging and hence possible nucleation and expansion of pores could not be detected if fusion occurred at sub-millisecond time scales as was observed for GUV–GUV fusion in [37] (see figure 4).

Pulsed lasers operate by delivering nanosecond or femto-second energy pulses in a highly focused Gaussian shaped focal region. The lateral and axial extents of the focal intensity distribution have a full width of half maximum of ~500 nm for near infrared light but somewhat smaller for ultraviolet laser light. Nanosecond pulses can ionize the biological material, but also cause shock waves and cavitation formation which extend beyond the focus and thus perturb biological structures [117]. Femtosecond lasers create an extremely transient

electronic plasma of the biological material confined at a scale below the diffraction limit, thus disrupting the biological structures with high precision [52, 118]. After the exposure the bilayer is found to reassemble into a hemifused [55, 114] or a fully fused bilayer structure [53]. Energy deposition can be significantly increased by irradiating absorbing plasmonic GNPs located at the contact region between the membranes. Irradiation of GNPs by fs pulsed lasers causes shock waves emanating from the GNPs which can perturb the membranes locally [65, 66].

The energy needed for disrupting the membranes can also be delivered by photothermal heating as is the case for hot-nanoparticle-mediated fusion. Irradiation of GNPs using a CW laser trap causes extremely local temperature rises of

~100 °C and can cause drastic effects on membranes, in particular near phase transitions [23, 34, 35, 68, 82, 100, 119, 120]. Membranes of cells exist mostly in a fluid state and the temperature induced expansion of fluid phase membranes has been measured and is found to have an area expansion of 0.5%/K [99]. The high local temperature rises will therefore inevitably disrupt membranes.

Important for fusion involving cells is the fact that cells have ruffled surfaces, and additionally stiff protrusive structures like filopodia which might prevent sufficiently close contact for enabling fusion. In some of the studies listed in table 2 treating cells with hypotonic medium prior to fusion is found to improve the fusion efficiency. A detailed study of the effect of osmolarity was conducted in [47, 50]. The benefit of swelling the cells might well be explained by a flattening of the cell surface, thus allowing closer contact between the cells. Swelling also leads to higher membrane tensions which is known to lower the energy barrier for fusion [121].

Membrane vesicles are more susceptible to changes in osmotic pressure than cells. Small imbalances in osmolarity between the inside and outside medium largely affect the membrane tension and the probability for fusion [122]. A more controlled way of controlling membrane tension is to use the micropipette aspiration technique. This technique has been widely used in studying mechanical properties of membranes since it allows accurate control over membrane tension through adjustments of the pressure within the aspirating micropipette [123]. The aspiration technique has been used to bring two vesicles into close contact prior to chemically induced fusion [37, 122]. First, the GUVs were positioned in close proximity and secondly the nanoscale separation was tuned by adjusting the membrane tension. At high membrane tension the entropic membrane undulations become smeared-out and the inter-membrane distance decreases [124, 125]. This effect can be effectively observed in fusion mediated by cognate SNARE proteins on apposing membranes where molecular interactions can only occur once a critical distance, corresponding to the range of SNAREs (8 nm), is reached. By increasing the membrane tension, SNARE mediated adhesion between membranes could be controlled prior to fusion as shown in [124].

### 5.2. Cell pairing

The fusion efficiency can be greatly improved by properly pairing cells prior to application of a physical trigger of fusion. The recent developments in microstructure fabrication combined with microfluidics have had immense impact how cells can be controllably paired in large arrays of cell traps [33]. The weakness of such approaches is the lack of selectivity of which specific cells to fuse. If specific cells need to be chosen in a population of cells it is recommended to use optical traps for pairing cells [22, 26]. High throughput techniques for cell pairing create large numbers of hybrid cells and hence it becomes relevant to introduce techniques for sorting the fraction of fused cells from unfused cells. This could be achieved by using fluorescent based sorting techniques if hybrid cells were labeled with different fluorophores than unfused cells.

## 6. Summary and future directions

Optically controlled fusion has proven to be a useful alternative to chemically induced fusion mediated by PEG polymers. A large number of different cell types and membrane vesicles can produce viable fused structures using electrofusion and optical based methods. We expect that fusion of cells will be a fruitful tool in research areas involving, for instance, stem cell research in the context of cellular reprogramming.

More detailed studies are needed to delineate the long term fate of hybrid cells and to determine if nuclear fusion can be brought to occur. Polynucleated cells do exist in biology and in many fusion experiments such cells are found [50]. The long-term survival of such cells would be interesting to follow.

Biophysical studies of membranes might benefit from the single cell approaches reviewed here. Fusion of single vesicles allows control over membrane compositions and the content of vesicles and cells. This will likely open up a range of new experimental approaches for investigating biological chemistry at pico-liter scale.

The different techniques used in optically triggered fusion have the potential to be used in other less biological structures. This was recently demonstrated in [41] where GNP modified polyelectrolyte capsules were fused using a laser.

Recent developments in simultaneous optical trapping of several cells, using holographic optical techniques, provides exciting possibilities for fusion which could become optically controlled by fully integrated robotics. To realize this, trapping of multiple cells, held in close proximity, first needs to be combined with a laser mediated fusion scheme, like fs pulsed laser, mediated fusion. Such experiments have so far not been realized, but should be within reach with the major technological developments seen in optical manipulation and biophotonics in the past decade [26, 126–129].

## Acknowledgments

This work was funded by the Danish Council for Independent Research (grant: DFF—4181-00196), the Novo Nordisk Foundation (grant: NNF14OC0011361), the Danish Research Council's Elite Research Prize (grant: 4094-00057B) and Danish National Research Foundation (grant: DNRF116).

## ORCID iDs

Lene B Oddershede  <https://orcid.org/0000-0003-2923-2844>  
Poul M Bendix  <https://orcid.org/0000-0001-8838-8887>

## References

- [1] Martens S and McMahon H T 2008 Mechanisms of membrane fusion: disparate players and common principles *Nat. Rev. Mol. Cell Biol.* **9** 543–56
- [2] Vassilopoulos G, Wang P R and Russell D W 2003 Transplanted bone marrow regenerates liver by cell fusion *Nature* **422** 901–4

- [3] Bahadori A, Lund A R, Semsey S, Oddershede L B and Bendix P M 2016 Controlled cellular fusion using optically trapped plasmonic nano-heaters *Proc. SPIE* **9922** 992211
- [4] Rorvig-Lund A, Bahadori A, Semsey S, Bendix P M and Oddershede L B 2015 Vesicle fusion triggered by optically heated gold nanoparticles *Nano Lett.* **15** 4183–8
- [5] Dimova R *et al* 2009 Vesicles in electric fields: some novel aspects of membrane behavior *Soft Matter* **5** 3201–12
- [6] Wernig M *et al* 2007 *In vitro* reprogramming of fibroblasts into a pluripotent ES-cell-like state *Nature* **448** 318–2
- [7] Cowan C A, Atienza J, Melton D A and Eggan K 2005 Nuclear reprogramming of somatic cells after fusion with human embryonic stem cells *Science* **309** 1369–73
- [8] Ambrosi D J and Rasmussen T P 2005 Reprogramming mediated by stem cell fusion *J. Cell. Mol. Med.* **9** 320–30
- [9] Tada M, Tada T, Lefebvre L, Barton S C and Surani M A 1997 Embryonic germ cells induce epigenetic reprogramming of somatic nucleus in hybrid cells *EMBO J.* **16** 6510–20
- [10] Saito A C, Ogura T, Fujiwara K, Murata S and Nomura S M 2014 Introducing micrometer-sized artificial objects into live cells: a method for cell-giant unilamellar vesicle electrofusion *PLoS One* **9** e106853
- [11] Robinson T, Verboket P E, Eyer K and Dittrich P S 2014 Controllable electrofusion of lipid vesicles: initiation and analysis of reactions within biomimetic containers *Lab Chip* **14** 2852–9
- [12] Steubing R W, Cheng S, Wright W H, Numajiri Y and Berns M W 1991 Laser induced cell fusion in combination with optical tweezers: the laser cell fusion trap *Cytometry* **12** 505–10
- [13] Wiegand R *et al* 1987 Laser-induced fusion of mammalian-cells and plant-protoplasts *J. Cell Sci.* **88** 145–9
- [14] Weissleder R 2001 A clearer vision for *in vivo* imaging *Nat. Biotechnol.* **19** 316–7
- [15] Svoboda K and Block S M 1994 Biological applications of optical forces *Annu. Rev. Biophys. Biomol.* **23** 247–85
- [16] Ashkin A, Dziedzic J M and Yamane T 1987 Optical trapping and manipulation of single cells using infrared-laser beams *Nature* **330** 769–71
- [17] Neuman K C, Chadd E H, Liou G F, Bergman K and Block S M 1999 Characterization of photodamage to *Escherichia coli* in optical traps *Biophys. J.* **77** 2856–63
- [18] Rasmussen M B, Oddershede L B and Siegmundfeldt H 2008 Optical tweezers cause physiological damage to *Escherichia coli* and *Listeria* bacteria *Appl. Environ. Microb.* **74** 2441–6
- [19] Norregaard K, Metzler R, Ritter C M, Berg-Sorensen K and Oddershede L B 2017 Manipulation and motion of organelles and single molecules in living cells *Chem. Rev.* **117** 4342–75
- [20] Chen S X *et al* 2013 Laser induced fusion of human embryonic stem cells with optical tweezers *Appl. Phys. Lett.* **103** 033701
- [21] Bendix P M and Oddershede L B 2011 Expanding the optical trapping range of lipid vesicles to the nanoscale *Nano Lett.* **11** 5431–7
- [22] Bahadori A, Oddershede L and Bendix P 2017 Hot-nanoparticle-mediated fusion of selected cells *Nano Res.* **10** 2034–45
- [23] Andersen T *et al* 2014 Nanoscale phase behavior on flat and curved membranes *Nanotechnology* **25** 505101
- [24] Reicherter M, Haist T, Wagemann E U and Tiziani H J 1999 Optical particle trapping with computer-generated holograms written on a liquid-crystal display *Opt. Lett.* **24** 608–10
- [25] Mogensen P C and Gluckstad J 2000 Dynamic array generation and pattern formation for optical tweezers *Opt. Commun.* **175** 75–81
- [26] Kirkham G R *et al* 2015 Precision assembly of complex cellular microenvironments using holographic optical tweezers *Sci. Rep.* **5** 8577
- [27] Perez-Vargas J *et al* 2014 Structural basis of eukaryotic cell-cell fusion *Cell* **157** 407–19
- [28] Chernomordik L V and Kozlov M M 2008 Mechanics of membrane fusion *Nat. Struct. Mol. Biol.* **15** 675–83
- [29] Milstein C 1999 The hybridoma revolution: an offshoot of basic research *Bioessays* **21** 966–73
- [30] Pan G J, Wang T, Yao H J and Pei D Q 2012 Somatic cell reprogramming for regenerative medicine: SCNT versus iPS cells *Bioessays* **34** 472–6
- [31] Wilmut I, Schnieke A E, McWhir J, Kind A J and Campbell K H S 1997 Viable offspring derived from fetal and adult mammalian cells *Nature* **385** 810–3
- [32] Takahashi K and Yamanaka S 2006 Induction of pluripotent stem cells from mouse embryonic and adult fibroblast cultures by defined factors *Cell* **126** 663–76
- [33] Skelley A M, Kirak O, Suh H, Jaenisch R and Voldman J 2009 Microfluidic control of cell pairing and fusion *Nat. Methods* **6** 147–52
- [34] Andersen T, Kyrsting A and Bendix P M 2014 Local and transient permeation events are associated with local melting of giant liposomes *Soft Matter* **10** 4268–74
- [35] Bendix P M, Reihani S N and Oddershede L B 2010 Direct measurements of heating by electromagnetically trapped gold nanoparticles on supported lipid bilayers *ACS Nano* **4** 2256–62
- [36] Yang P, Lipowsky R and Dimova R 2009 Nanoparticle formation in giant vesicles: synthesis in biomimetic compartments *Small* **5** 2033–7
- [37] Haluska C K *et al* 2006 Time scales of membrane fusion revealed by direct imaging of vesicle fusion with high temporal resolution *Proc. Natl Acad. Sci. USA* **103** 15841–6
- [38] Prevost C *et al* 2015 IRSp53 senses negative membrane curvature and phase separates along membrane tubules *Nat. Commun.* **6** 8529
- [39] Carvalho K *et al* 2013 Cell-sized liposomes reveal how actomyosin cortical tension drives shape change (vol 110, pg 16456, 2013) *Proc. Natl Acad. Sci. USA* **110** 19969
- [40] Aimon S *et al* 2014 Membrane shape modulates transmembrane protein distribution *Dev. Cell* **28** 212–8
- [41] Wu Y, Frueh J, Si T, Mohwald H and He Q 2015 Laser-induced fast fusion of gold nanoparticle-modified polyelectrolyte microcapsules *Phys. Chem. Chem. Phys.* **17** 3281–6
- [42] Zhang P *et al* 2014 Preparation of triple-negative breast cancer vaccine through electrofusion with day-3 dendritic cells *PLoS One* **9** e102197
- [43] Kanduser M and Usaj M 2014 Cell electrofusion: past and future perspectives for antibody production and cancer cell vaccines *Exp. Opin. Drug Deliv.* **11** 1885–98
- [44] Yanai G *et al* 2013 Electrofusion of mesenchymal stem cells and islet cells for diabetes therapy: a rat model *PLoS One* **8** e64499
- [45] Usaj M, Flisar K, Miklavcic D and Kanduser M 2013 Electrofusion of B16-F1 and CHO cells: the comparison of the pulse first and contact first protocols (vol 89, pg 34, 2013) *Bioelectrochemistry* **92** 47
- [46] Rems L *et al* 2013 Cell electrofusion using nanosecond electric pulses *Sci. Rep.* **3** 3382
- [47] Usaj M, Trontelj K, Miklavcic D and Kanduser M 2010 Cell-cell electrofusion: optimization of electric field amplitude and hypotonic treatment for mouse melanoma (B16-F1) and chinese hamster ovary (CHO) cells *J. Membr. Biol.* **236** 107–16
- [48] Stromberg A *et al* 2000 Manipulating the genetic identity and biochemical surface properties of individual cells with

- electric-field-induced fusion *Proc. Natl Acad. Sci. USA* **97** 7–11
- [49] Wang X L *et al* 2011 Enhanced cell sorting and manipulation with combined optical tweezer and microfluidic chip technologies *Lab Chip* **11** 3656–62
- [50] Usaj M and Kanduser M 2012 The systematic study of the electroporation and electrofusion of B16-F1 and CHO cells in isotonic and hypotonic buffer *J. Membr. Biol.* **245** 583–90
- [51] Greulich K O 2017 Manipulation of cells with laser microbeam scissors and optical tweezers: a review *Rep. Prog. Phys.* **80** 026601
- [52] Katchinskiy N, Godbout R and Elezzabi A Y 2016 Characterization of femtosecond-laser pulse induced cell membrane nanosurgical attachment *Biomed. Opt. Express* **7** 2749–58
- [53] Kuetemeyer K, Lucas-Hahn A, Petersen B, Niemann H and Heisterkamp A 2011 Femtosecond laser-induced fusion of nonadherent cells and two-cell porcine embryos *J. Biomed. Opt.* **16** 088001
- [54] He H, Chan K T, Kong S K and Lee R K Y 2008 All-optical human cell fusion by a fiber femtosecond laser *Appl. Phys. Lett.* **93** 163901
- [55] Katchinskiy N, Goez H R, Dutta I, Godbout R and Elezzabi A Y 2016 Novel method for neuronal nanosurgical connection *Sci. Rep.* **6** 20529
- [56] Vogel A, Noack J, Huttman G and Paltauf G 2005 Mechanisms of femtosecond laser nanosurgery of cells and tissues *Appl. Phys. B* **81** 1015–47
- [57] Antkowiak M *et al* 2013 Fast targeted gene transfection and optogenetic modification of single neurons using femtosecond laser irradiation *Sci. Rep.* **3** 3281
- [58] Truong T V, Supatto W, Koos D S, Choi J M and Fraser S E 2011 Deep and fast live imaging with two-photon scanned light-sheet microscopy *Nat. Methods* **8** 757–60
- [59] Stacey M, Fox P, Buescher S and Kolb J 2011 Nanosecond pulsed electric field induced cytoskeleton, nuclear membrane and telomere damage adversely impact cell survival *Bioelectrochemistry* **82** 131–4
- [60] Mohanty S K, Sharma M and Gupta P K 2006 Generation of ROS in cells on exposure to CW and pulsed near-infrared laser tweezers *Photochem. Photobiol. Sci.* **5** 134–9
- [61] Tirlapur U K, König K, Peuckert C, Krieg R and Halhuber K J 2001 Femtosecond near-infrared laser pulses elicit generation of reactive oxygen species in mammalian cells leading to apoptosis-like death *Exp. Cell Res.* **263** 88–97
- [62] Wang R *et al* 2016 Fusion with stem cell makes the hepatocellular carcinoma cells similar to liver tumor-initiating cells *BMC Cancer* **16** 56
- [63] Ichikawa M and Yoshikawa K 2001 Optical transport of a single cell-sized liposome *Appl. Phys. Lett.* **79** 4598–600
- [64] Yao C *et al* 2005 Elevation of plasma membrane permeability by laser irradiation of selectively bound nanoparticles *J. Biomed. Opt.* **10** 064012
- [65] Yeheskely-Hayon D, Minai L, Golan L, Dann E J and Yelin D 2013 Optically induced cell fusion using bispecific nanoparticles *Small* **9** 3771–7
- [66] Minai L *et al* 2012 Optical nanomanipulations of malignant cells: controlled cell damage and fusion *Small* **8** 1732–9
- [67] Bohren C F and Huffman D R 1983 *Absorption and Scattering of Light by Small Particles* (New York: Wiley)
- [68] Kyrsting A, Bendix P M, Stamou D G and Oddershede L B 2011 Heat profiling of three-dimensionally optically trapped gold nanoparticles using vesicle cargo release *Nano Lett.* **11** 888–92
- [69] Seol Y, Carpenter A E and Perkins T T 2006 Gold nanoparticles: enhanced optical trapping and sensitivity coupled with significant heating *Opt. Lett.* **31** 2429–31
- [70] Ruijgrok P V, Verhart N R, Zijlstra P, Tchegobtareva A L and Orrit M 2011 Brownian fluctuations and heating of an optically aligned gold nanorod *Phys. Rev. Lett.* **107** 037401
- [71] Hansen P M, Bhatia V K, Harrit N and Oddershede L 2005 Expanding the optical trapping range of gold nanoparticles *Nano Lett.* **5** 1937–42
- [72] Hajizadeh F and Reihani S N S 2010 Optimized optical trapping of gold nanoparticles *Opt. Express* **18** 551–9
- [73] Qin Z and Bischof J C 2012 Thermophysical and biological responses of gold nanoparticle laser heating *Chem. Soc. Rev.* **41** 1191–217
- [74] Svoboda K and Block S M 1994 Optical trapping of metallic Rayleigh particles *Opt. Lett.* **19** 930–2
- [75] Zensen C, Villadsen N, Winterer F, Keiding S R and Lohmüller T 2016 Pushing nanoparticles with light—a femtonewton resolved measurement of optical scattering forces *APL Photonics* **1** 026102
- [76] Fedoruk M, Meixner M, Carretero-Palacios S, Lohmüller T and Feldmann J 2013 Nanolithography by plasmonic heating and optical manipulation of gold nanoparticles *ACS Nano* **7** 7648–53
- [77] Dienerowitz M, Mazilu M, Reece P J, Krauss T F and Dholakia K 2008 Optical vortex trap for resonant confinement of metal nanoparticles *Opt. Express* **16** 4991–9
- [78] Osinkina L *et al* 2013 Tuning DNA binding kinetics in an optical trap by plasmonic nanoparticle heating *Nano Lett.* **13** 3140–4
- [79] Kyrsting A, Bendix P M and Oddershede L B 2013 Mapping 3D focal intensity exposes the stable trapping positions of single nanoparticles *Nano Lett.* **13** 31–5
- [80] Ohlinger A, Deak A, Lutich A A and Feldmann J 2012 Optically trapped gold nanoparticle enables listening at the microscale *Phys. Rev. Lett.* **108** 018101
- [81] Guffey M J and Scherer N F 2010 All-optical patterning of Au nanoparticles on surfaces using optical traps *Nano Lett.* **10** 4302–8
- [82] Jorgensen J T *et al* 2016 Single particle and pet-based platform for identifying optimal plasmonic nano-heaters for photothermal cancer therapy *Sci. Rep.* **6** 30076
- [83] Baffou G *et al* 2013 Photoinduced heating of nanoparticle arrays *ACS Nano* **7** 6478–88
- [84] Brzobohaty O *et al* 2015 Three-dimensional optical trapping of a plasmonic nanoparticle using low numerical aperture optical tweezers *Sci. Rep.* **5** 8106
- [85] Bosanac L, Aabo T, Bendix P M and Oddershede L B 2008 Efficient optical trapping and visualization of silver nanoparticles *Nano Lett.* **8** 1486–91
- [86] Blattmann M and Rohrbach A 2015 Plasmonic coupling dynamics of silver nanoparticles in an optical trap *Nano Lett.* **15** 7816–21
- [87] Tanaka Y, Yoshikawa H, Itoh T and Ishikawa M 2009 Surface enhanced raman scattering from pseudoisocyanine on Ag nanoaggregates produced by optical trapping with a linearly polarized laser beam *J. Phys. Chem. C* **113** 11856–60
- [88] Ohlinger A, Nedev S, Lutich A A and Feldmann J 2011 Optothermal escape of plasmonically coupled silver nanoparticles from a three-dimensional optical trap *Nano Lett.* **11** 1770–4
- [89] Svedberg F, Li Z P, Xu H X and Kall M 2006 Creating hot nanoparticle pairs for surface-enhanced Raman spectroscopy through optical manipulation *Nano Lett.* **6** 2639–41
- [90] Selhuber-Unkel C, Zins I, Schubert O, Sonnichsen C and Oddershede L B 2008 Quantitative optical trapping of single gold nanorods *Nano Lett.* **8** 2998–3003
- [91] Pelton M *et al* 2006 Optical trapping and alignment of single gold nanorods by using plasmon resonances *Opt. Lett.* **31** 2075–7

- [92] Toussaint K C *et al* 2007 Plasmon resonance-based optical trapping of single and multiple Au nanoparticles *Opt. Express* **15** 12017–29
- [93] Ma H Y, Bendix P M and Oddershede L B 2012 Large-scale orientation dependent heating from a single irradiated gold nanorod *Nano Lett.* **12** 3954–60
- [94] Baffou G, Kreuzer M P, Kulzer F and Quidant R 2009 Temperature mapping near plasmonic nanostructures using fluorescence polarization anisotropy *Opt. Express* **17** 3291–8
- [95] Bendix P M, Jauffred L, Norregaard K and Oddershede L B 2014 Optical trapping of nanoparticles and quantum dots *IEEE J. Sel. Top. Quantum Electron.* **20** 4800112
- [96] Hester B *et al* 2012 Tunable optical tweezers for wavelength-dependent measurements *Rev. Sci. Instrum.* **83** 043114
- [97] Lasic D D 1998 Novel applications of liposomes *Trends Biotechnol.* **16** 307–21
- [98] Angelova M I and Dimitrov D S 1986 Liposome electroformation *Faraday Discuss.* **81** 303
- [99] Pan J *et al* 2012 Molecular structures of fluid phase phosphatidylglycerol bilayers as determined by small angle neutron and x-ray scattering *Biochim. Biophys. Acta* **1818** 2135–48
- [100] Schuy S and Janshoff A 2006 Thermal expansion of microstructured DMPC bilayers quantified by temperature-controlled atomic force microscopy *ChemPhysChem* **7** 1207–10
- [101] Peters R, Peters J, Tews K H and Bahr W 1974 A microfluorimetric study of translational diffusion in erythrocyte membranes *Biochim. Biophys. Acta* **367** 282–94
- [102] Rawle R J, van Lengerich B, Chung M, Bendix P M and Boxer S G 2011 Vesicle fusion observed by content transfer across a tethered lipid bilayer *Biophys. J.* **101** L37–39
- [103] Luby-Phelps K 2000 Cytoarchitecture and physical properties of cytoplasm: volume, viscosity, diffusion, intracellular surface area *Int. Rev. Cytol.* **192** 189–221
- [104] Stockert J C, Blazquez-Castro A, Canete M, Horobin R W and Villanueva A 2012 MTT assay for cell viability: Intracellular localization of the formazan product is in lipid droplets *Acta Histochem.* **114** 785–96
- [105] Liu Y B, Peterson D A, Kimura H and Schubert D 1997 Mechanism of cellular 3-(4,5-dimethylthiazol-2-yl)-2,5-diphenyltetrazolium bromide (MTT) reduction *J. Neurochem.* **69** 581–93
- [106] Ren G, Vajihala P, Lee J S, Winsor B and Munn A L 2006 The BAR domain proteins: molding membranes in fission, fusion, and phagy *Microbiol. Mol. Biol. Rev.* **70** 37–120
- [107] Derganc J, Antonny B and Copic A 2013 Membrane bending: the power of protein imbalance *Trends Biochem. Sci.* **38** 576–84
- [108] Stachowiak J C *et al* 2012 Membrane bending by protein-protein crowding *Nat. Cell Biol.* **14** 944–9
- [109] Lingwood D, Ries J, Schwille P and Simons K 2008 Plasma membranes are poised for activation of raft phase coalescence at physiological temperature *Proc. Natl Acad. Sci. USA* **105** 10005–10
- [110] Sezgin E *et al* 2012 Elucidating membrane structure and protein behavior using giant plasma membrane vesicles *Nat. Protocols* **7** 1042–51
- [111] Maruyama H, Inoue N, Masuda T and Arai F 2011 Selective injection and laser manipulation of nanotool inside a specific cell using optical ph regulation and optical tweezers *IEEE Int. Conf. Robotics and Automation* pp 2674–9
- [112] Shirakashi R, Sukhorukov V L, Reuss R, Schulz A and Zimmermann U 2012 Effects of a pulse electric field on electrofusion of giant unilamellar vesicle (GUV)-jurkat cell (measurement of fusion ratio and electric field analysis of pulsed guv-jurkat cell) *J. Therm. Sci. Technol. Japan* **7** 589–602
- [113] Yang P F, Wang C H and Lee G B 2016 Optically-induced cell fusion on cell pairing microstructures *Sci. Rep.* **6** 22036
- [114] Katchinsky N, Godbout R, Goetz H R and Elezabi A Y 2014 Femtosecond laser-induced cell–cell surgical attachment *Laser Surg. Med.* **46** 335–41
- [115] Gatti R *et al* 1998 Comparison of annexin V and calcein-AM as early vital markers of apoptosis in adherent cells by confocal laser microscopy *J. Histochem. Cytochem.* **46** 895–900
- [116] Kaneshiro E S, Wyder M A, Wu Y-P and Cushion M T 1993 Reliability of calcein acetoxy methyl ester and ethidium homodimer or propidium iodide for viability assessment of microbes *J. Microbiol. Methods* **17** 1–16
- [117] Venugopalan V, Guerra A III, Nahen K and Vogel A 2002 Role of laser-induced plasma formation in pulsed cellular microsurgery and micromanipulation *Phys. Rev. Lett.* **88** 078103
- [118] Sacconi L, Tolic-Norrelykke I M, Antolini R and Pavone F S 2005 Combined intracellular three-dimensional imaging and selective nanosurgery by a nonlinear microscope *J. Biomed. Opt.* **10** 14002
- [119] Urban P, Kirchner S R, Muhlbauer C, Lohmuller T and Feldmann J 2016 Reversible control of current across lipid membranes by local heating *Sci. Rep.* **6** 22686
- [120] Urban A S *et al* 2009 Controlled nanometric phase transitions of phospholipid membranes by plasmonic heating of single gold nanoparticles *Nano Lett.* **9** 2903–8
- [121] Kim J H *et al* 2015 Mechanical tension drives cell membrane fusion *Dev. Cell* **32** 561–73
- [122] Lipowsky R *et al* 2005 Wetting, budding, and fusion-morphological transitions of soft surfaces *J. Phys.: Condens. Matter* **17** S2885–902
- [123] Evans E and Yeung A 1989 Apparent viscosity and cortical tension of blood granulocytes determined by micropipet aspiration *Biophys. J.* **56** 151–60
- [124] Warner J M, Karatekin E and O’Shaughnessy B 2009 Model of SNARE-mediated membrane adhesion kinetics *PLoS One* **4** e6375
- [125] Radler J O, Feder T J, Strey H H and Sackmann E 1995 Fluctuation analysis of tension-controlled undulation forces between giant vesicles and solid substrates *Phys. Rev. E* **51** 4526–36
- [126] Dholakia K and Cizmar T 2011 Shaping the future of manipulation *Nat. Photon.* **5** 335–42
- [127] Kim K and Park Y 2017 Tomographic active optical trapping of arbitrarily shaped objects by exploiting 3D refractive index maps *Nat. Commun.* **8** 15340
- [128] Hu S Y and Sun D 2011 Automatic transportation of biological cells with a robot-tweezer manipulation system *Int. J. Robot. Res.* **30** 1681–94
- [129] Chiou P Y, Ohta A T and Wu M C 2005 Massively parallel manipulation of single cells and microparticles using optical images *Nature* **436** 370–2



**Azra Bahadori** received her PhD degree at the Niels Bohr Institute in 2016. During her PhD she worked extensively with fusion of vesicles and cells using plasmonic heating. She worked as a postdoc at the Niels Bohr Institute from 2016--2017 where she investigated biophysical aspects of the cell surface using fluorescence microscopy and plasmonic heating.



**Guillermo Moreno-Pescador** received his MSc degree in Physics in 2015 from the University of Copenhagen, Denmark. Currently, he is a PhD candidate at the Niels Bohr Institute in Experimental Biophysics. His research focuses on the study of motility of membrane proteins in native membrane models. His research interests include acoustics, cell migration and membrane fusion.



**Lene Broeng Oddershede** is a Professor of Experimental Physics at the Niels Bohr Institute, University of Copenhagen, Denmark. She is also Center Leader for StemPhys Center of Excellence. She is well known for her work on optical manipulation of nanoparticles and single molecules, also inside living cells.



**Poul Martin Bendix** is an Associate Professor in experimental physics at the Niels Bohr Institute. His main research interests include biophysics and dynamics of cells surface structures and associated proteins. Also, he has worked extensively with interactions between light and nanoparticles with respect to both heating and trapping. He received the Young Investigator Award in 2011 from the Villum Foundation and in 2015 he received the Sapere Aude research leader grant from the Danish Council for Independent Research.